universität wien

MASTERARBEIT / MASTER'S THESIS

Titel der Masterarbeit / Title of the Master's Thesis

„Influence of sugar consumption on fat storage and intestinal barrier function: Studies in *Caenorhabditis elegans* "

verfasst von / submitted by

Elisabeth Kaufmann, BSc

angestrebter akademischer Grad / in partial fulfilment of the requirements for the degree of

Master of Science (MSc)

Wien, 2019 / Vienna, 2019

Studienkennzahl lt. Studienblatt / degree programme code as it appears on the student record sheet:	A 066 838
Studienrichtung lt. Studienblatt / degree programme as it appears on the student record sheet:	Ernährungswissenschaften / Nutritional Sciences
Betreut von / Supervisor:	Univ.-Prof. Dipl. oec. troph. Dr. Ina Bergheim

Acknowledgments

I wish to express my deep gratitude to my supervisor Professor Dr. Ina Bergheim for providing me the opportunity to conduct this study, her useful comments, constructive remarks, contiguous encouragement, and patience.

My sincere thanks also go to Dragana Rajcic for always being supportive of my work.

The guidance provided by Janina Engstler was also greatly appreciated.

My thanks are extended to all members of the working group, namely Anja Baumann, Finn Jung, Annette Brandt, Anika Nier, and Beate Gärtner, for their advice and support during the time of the study and beyond.

I also wish to acknowledge my colleagues Esther Pilar, Andrea Leitner, Eva-Maria Stix, Stefanie Holper, and Vincent Winkler for the stimulating discussions and uplifting talks.

Finally, I would like to thank my parents for their financial support and patience.

Content

Figures

Tables

Abbreviations

AJ	adherens junction
AJM-1	apical junction molecule 1
AMP	adenosine monophosphate
AMPK	AMP-activated kinase
ANOVA	analysis of variance
4-AP	4-aminophenazone
ATP	adenosine triphosphate
BSA	bovine serum albumin
C	control
$CaCl_2•2H_2O$	calcium chloride dihydrate
CCC	cadherin-catenin complex
CeAJ	*C. elegans* apical junction
ChREBP	carbohydrate responsive element-binding protein
4-CP	4-chlorphenol
C_T	cycle threshold
cDNA	complementary DNA
ddH_2O	distilled, deionized water
DAG	diacylglycerol
DAC	DLG-1/AJM-1 complex
DF	dilution factor
DHAP	dihydroxy acetone phosphate
DLG-1	Discs large homolog 1
DNA	deoxynucleic acid
DNL	*de novo* lipogenesis
EDTA	ethylenediamine tetra acetic acid
FA	fatty acids
FFA	free fatty acids
F25	25 mM of fructose
F50	50 mM of fructose
G25	25 mM of glucose
G50	50 mM of glucose

GK	glucokinase
GKRP	GK regulatory protein
GLUT5	glucose transporter 5
G3P	glycerol-3-phosphate
GPO	glycerol-3-phosphate oxidase
HFCS	high-fructose corn syrup
4-HNL	4-hydroxynonenal
IGF-1	insulin-like growth factor 1
IκB	inhibitor of NFκB
iNOS	inducible NO synthase
IR	insulin receptor
JAK	Janus kinase
KCl	potassium chloride
KH_2PO_4	potassium dihydrogen phosphate
$K_2HPO_4•3H_2O$	potassium phosphate dibasic trihydrate
LB	lysogeny broth
LD	lipid droplets
LPL	lipoprotein lipase
LPS	lipopolysaccharide
MAPK	mitogen-activated protein kinase
$MgSO_4$	magnesium sulfate
mRNA	messenger RNA
mtROS	mitochondrial ROS
MyD88	myeloid differentiation primary response 88
Na_2HPO_4	disodium hydrogen phosphate
NaCl	sodium chloride
NAFLD	non-alcoholic fatty liver disease
NFκB	nuclear factor ‘kappa-light-chain-enhancer’ of activated B cells
NGM	nematode growth media
ORO	Oil red O
PBMC	peripheral blood mononuclear cells
PBS	phosphate buffered saline
PCR	polymerase chain reaction
Pi	inorganic phosphate

PFK-1	phosphofructokinase 1
PKCε	protein kinase Cε
POD	peroxidase
rcf	relative centrifugal force
RCT	randomized controlled trail
RFU	relative fluorescence units
RNA	ribonucleic acid
rRNA	ribosomal RNA
ROS	reactive oxygen species
RT-qPCR	real-time quantitative PCR
RQ	RNA-qualified
SCFA	short-chain fatty acids
SGLT-1	Na^+-D-glucose cotransporter-1
SI	supplementary information
SREBP-1c	sterol regulatory element-binding protein 1c
STAT	signal transducer and activator of transcription
TCA	tricarboxylic acid
TG	triglycerides
TGF	terminal growth factor
TJ	tight junction
TLR4	Toll-like receptor 4
TNFα	tumor necrosis factor α
TNFR1	TNFα receptor 1
TOR	target of rapamycin
TRIS	tris(hydroxymethyl)-aminomethane
UPR	unfolded protein response
WHO	World Health Organization
XBP1	X-box binding protein 1
YA	young adults
ZO-1	*zonula occludens* 1
ZOO-1	*zonula occludens* ortholog 1

1.Introduction

1.1. Fructose: Metabolism and associated alternations

Current estimates for the mean intake of mono- and disaccharides, added to foods and beverages during processing but also naturally present in honey, fruit juices, and fruit juice concentrates ('free sugars'), are 16.4 % and 17.5 % of total energy intake in Austrian men and women, respectively, with the top consumers ingesting more than 30.2 % and 29.8 % of their daily calories as 'free sugars' (1). Accordingly, 88.8 % of Austrian women and 81.4 % of Austrian men exceed the recommendations of the World Health Organization (WHO) regarding sugar intake and even more so to reduce sugar intake to less than 10 % of daily calories (1,2). Meta-analyses basing calculations on randomized controlled trails (RCTs) in humans suggest that high sugar consumption is related to body weight gain (3) and cardiometabolic risk factors, including elevated serum lipids and blood pressure (4).

The predominant sugars added to foods and beverages in many Westernized countries are sucrose and high-fructose corn syrup (HFCS) (5). While sucrose constitutes to equal proportions of fructose and glucose, the relative proportion of fructose to glucose in commercially available HFCS is 42 to 58 % (HFCS-42) and 55 to 45 % (HFCS-55), respectively (for an overview, see ref. (5)). Despite the fact that fructose and glucose are both hexose sugars, their cellular absorption, distribution, and metabolism differs markedly (6). Indeed, while glucose absorption across the brush border membrane of the small intestinal epithelium is mediated by Na^+-coupled co-transport via SGLT1 (7), fructose uptake by enterocytes occurs by facilitated diffusion via GLUT5 (8), which has been shown to be induced by high fructose loads in rodents (9).

Studies indicate that in the intestinal cell, a significant proportion of fructose is catabolized to glucose and organic acids prior to being released into the portal circulation via basolaterally expressed GLUT2, whereas glucose passes mainly unmetabolized into the portal vein (10,11). After absorption into portal blood, the

majority an oral glucose load is disposed of in peripheral tissues, primarily muscle (12–14), while most of the ingested fructose, arriving via the portal vein, is taken up by the liver representing the main site of fructose metabolism in rodents (15) and humans (16).

Fructose- and glucose-metabolizing pathways in the liver are summarized in Figure 1 (for an overview, see ref. (17)). In brief, hepatic glucose metabolism is initiated by the phosphorylation of glucose to glucose-6-phosphate followed by the reversible isomerization to fructose-6-phosphat (for an overview, see ref. (18)). Glucokinase (GK), which catalyzes the initial step of glucose metabolism in the liver (19), is regulated by insulin at the level of transcription (20,21) and allosterically regulated by GK regulatory protein (GKRP) and metabolites of glucose metabolism (22). In contrast, the initial phosphorylation of fructose occurs on 1-position catalyzed by fructokinase (23), unregulated by insulin (24) and metabolites of fructose metabolism (25). Fructose-6-phosphate is subsequently phosphorylated to fructose-1,6-bisphosphate catalyzed by phosphofructokinase (PFK), which is allosterically regulated by hepatocellular adenosine triphosphate (ATP) and citrate level (26), while fructose-1-phosphate is split by liver aldolase to generate dihydroxyacetone phosphate and glyceraldehyde, bypassing the PFK regulatory step in glycolysis (27). At the triosephosphate level, fructose- and glucose-metabolizing pathways in the liver converge, and hexose carbons are channeled into glycolytic, gluconeogenetic, lipogenic or oxidative pathways (for an overview, see ref. (27)).

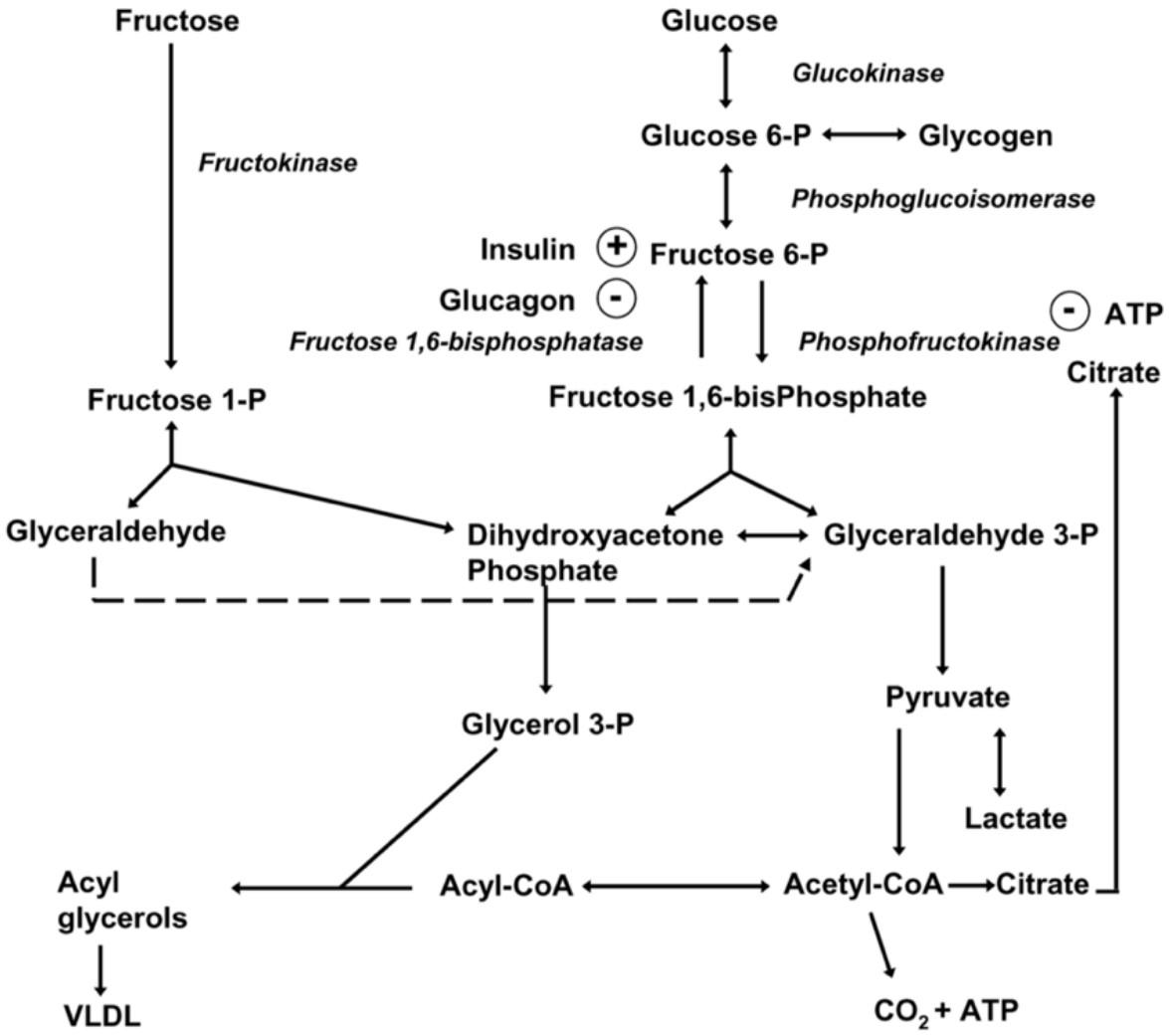

Figure 1: Fructose- and glucose-metabolizing pathways in the liver *(for an overview, see ref. (17)).*

1.2. Fructose consumption as a risk factor for the development of metabolic diseases

Fructose as substrate of hepatic de novo lipogenesis and potent inductor of lipogenic gene expression in the liver

Already more than 20 years ago, results of studies suggested that high fructose intake or bioavailability to the liver may add on elevated *de novo* lipogenesis (DNL) and the subsequent development of fatty liver (for an overview, see ref. (27)). Molecular mechanism linking hepatic fructose exposure to an induction of DNL in the liver are summarized in Figure 2 (for an overview, see ref. (28)).

In contrast to glucose, fructose utilization by the liver is unregulated by insulin and hepatocellular energy needs (6,15,24,29). Studies indicated that uncontrolled entry and metabolism of fructose in the liver may rapidly expand intrahepatic hexose- and triose-phosphate pool (30), increasing substrate availability relative to the oxidative capacities of the liver (31). In addition, it has been suggested that fructose or its metabolites may induce transcription factors of lipogenic and gluconeogenetic genes e.g. sterol regulatory element binding protein-1c (SREBP-1c) and carbohydrate-responsive element binding protein (ChREBP) (32,33), resulting in an upregulation of the expression of enzymes involved in fatty acid (FA) synthesis and glucose production in the liver (31–34). Furthermore, hepatic steatosis and hypertriglyceridemia induced by chronic intake of a diet rich in fructose have been related to a repression of transcription factors of genes involved in mitochondrial FA oxidation and inflammation e.g. peroxisome proliferator-activated receptor α (PPARα) (35). Indeed, evidence from RCTs in humans suggests that chronic, high fructose intake may result in an increase in DNL (36), reduced FA oxidation (37), and subclinical inflammation (38), while similar changes where not observed after long-term intake of a diet rich in glucose (36–38).

Moreover, rapid phosphorylation of fructose by fructokinase has been proposed to deplete liver adenosine triphosphate (ATP) and inorganic phosphate (Pi) (30,39). Studies in rodent models have shown that hepatocellular ATP and Pi depletion can

interfere with various energy-demanding processes in the liver, including ribonucleic acid (RNA) and protein synthesis (30,39). Elevated purine degradation may result in uric acid production (40) and a concomitant increase in mitochondrial reactive oxygen species (ROS) formation (41). Studies suggest that mitochondrial oxidative stress may inhibit key enzymes of the tricarboxylic acid (TCA) cycle, leading to citrate release into the cytosol and subsequent activation of enzymes involved in hepatic DNL e.g. FA synthase (FAS) (41).

In addition, fructose or its metabolites are assumed to promote DNL, at least in part, via the induction of endoplasmic reticulum (ER) stress and unfolded protein response (UPR) signaling in the liver (42,43). Indeed, presumed key regulators of the ER stress response were found to be upregulated in fructose-fed mice, associated with an increase in lipogenic gene expression and triglyceride (TG) accumulation in the liver (42–44).

It has been hypothesized, that fructose-induced increase in DNL may, in turn, promote hepatocellular diacylglycerol (DAG) accumulation (45) and DAG-dependent activation of protein kinase Cε (PKCε) (46), resulting in an impairment of hepatic insulin signaling (47) and the subsequent development of glucose intolerance and insulin resistance (36,48). In the state of hepatic insulin resistance, DNL is induced by insulin, while insulin-mediated suppression of glucose production is impaired, potentially leading to an exacerbation of hepatic steatosis, hyperlipidemia, and hyperglycemia (47,49).

Furthermore, evidence from RCTs in humans suggests that reduced postprandial insulin secretion after fructose consumption may promote visceral fat accumulation (36,50). Visceral adiposity is associated with a heightened expression of pro-inflammatory cytokines, which can potentially interfere with insulin signaling, resulting in adipose tissue lipolysis, and the concomitant increase in substrate supply for hepatic DNL (for an overview, see ref. (51)).

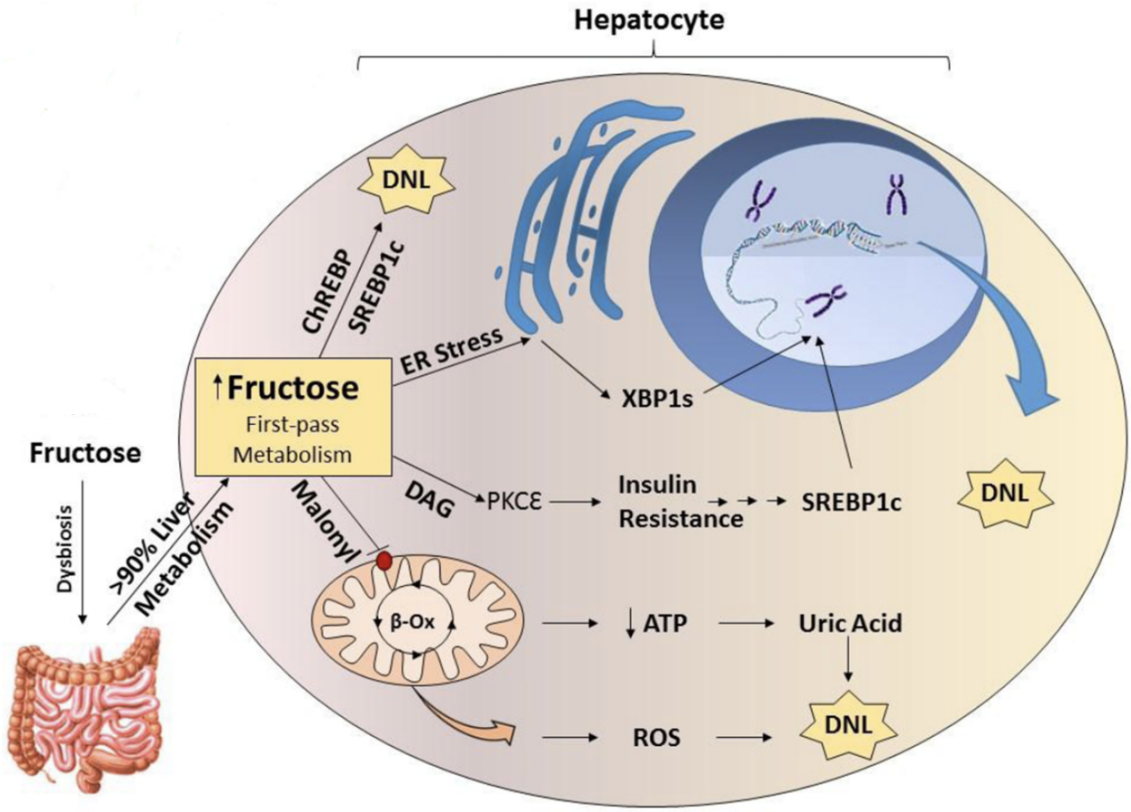

Figure 2: Molecular mechanism linking hepatic fructose exposure to elevated de novo lipogenesis *(for an overview, see ref. (28)). It is assumed, that the majority of an oral fructose load is disposed of by the liver (15,16). Hepatic fructose metabolism may not solely promote DNL by increasing substrate supply for FA synthesis and TG formation but also via the induction of ER stress, insulin resistance, ATP depletion, and mitochondrial ROS formation (for an overview, see ref. (28)). Abbreviations: ATP = adenosine triphosphate, ChREBP = carbohydrate-responsive binding protein, DAG = diacylglycerol, DNL = de novo lipogenesis, ER = endoplasmic reticulum, PKCε = protein kinase Cε, mtROS = mitochondrial reactive oxygen species, SREBP1c = sterol regulatory element binding protein 1c, XBP1s = X box binding protein 1s.*

Fructose as a modulator of gut microbiota composition and intestinal barrier function

Evidence from studies in higher animal models indicates that fructose-induced metabolic alternations may not solely result from its predominantly hepatic metabolism and highly lipogenic potential (52–54). Rather, elevated fructose intake may contribute to the development of fatty liver through a mechanism involving changes in gut microbiota composition and intestinal barrier (52) (for an overview, see ref. (55)).

Molecular mechanism linking intestinal barrier dysfunction to the development of non-alcoholic fatty liver disease (NAFLD) are summarized in Figure 3 (for comparison, see ref. (56)). Only recently, Jang *et al.* showed that higher doses of fructose are incompletely cleared by the small intestine and may thus elicit microbiota dysbiosis (10). Current evidence suggests that changes in gut microbiota composition, induced by diets high in sugar and herein particularly fructose can alter host physiology via multiple mechanism, including the fermentation of carbohydrates to short-chain fatty acids (SCFA) (57,58) as well as the modulation of bile acid homeostasis (59), alternations in gut-brain vagal communication (60), production of endogenous ethanol (61,62), and release of toxins, notably endotoxin (63,64) (for an overview, see ref. (65)).

Studies in rodent models of NAFLD have repeatedly shown that chronic intake of a diet high in fructose, but not glucose, is associated with alternations in gut microbiota composition (57,64) as well as a loss of tight junction (TJ) proteins in the upper parts of the small intestine (59,66), resulting in an elevated translocation of bacterial endotoxin into the portal vein and an induction of Toll-like receptor 4 (TLR-4)-dependent signaling cascades in the liver (54,67). In consistence, a recent human study showed that short-term intake of a diet high in fructose is sufficient to induce an increase in markers of liver damage, while similar changes were not observed after short-term intake of a diet high in glucose (68). Fructose-induced liver damage was further associated with a rise in circulating endotoxin levels as well as an induction of the TLR-4 signaling cascade in peripheral blood mononuclear cells (PBMCs) (68).

It is assumed, that the interaction of endotoxin with TLR-4 on hepatic Kupffer cells, possibly via activation of the TLR adapter protein myeloid differentiation primary response 88 (MyD88) (54) and upregulation of the inducible nitric oxide (NO) synthase (iNOS), may increase the formation of ROS (54), which, in turn, can promote the nuclear translocation of the transcription factor nuclear factor 'kappa-light-chain-enhancer' of activated B cells (NFκB), resulting in an up-regulation of the expression of pro-inflammatory cytokines such as tumor necrosis factor-α (TNF-α) (54). In consistence, 4-hydroxynonenal (4-HNE) adduct formation, inhibitor of NFκB (IκB) phosphorylation, and TNF-α mRNA expression in the livers of mice fed a high-fructose diet were found to be increased, while similar changes were not observed in mice fed a diet high in glucose (52,66).

Studies from Kanuri *et al.* suggest that TNF-α may either directly or indirectly e.g. through dysregulation of hepatic insulin signaling or suppression of AMPK activation in the liver add on elevated DNL and the subsequent development of NAFLD (53). In support of these mechanisms, fructose-fed mice treated with probiotics (57,58) or non-resorbable antibiotics (52), as well as both, TLR-4 mutant (54) and TNFR1 knockout mice (53), were found to be markedly protected from fructose-induced hepatic steatosis, inflammation, and oxidative damage.

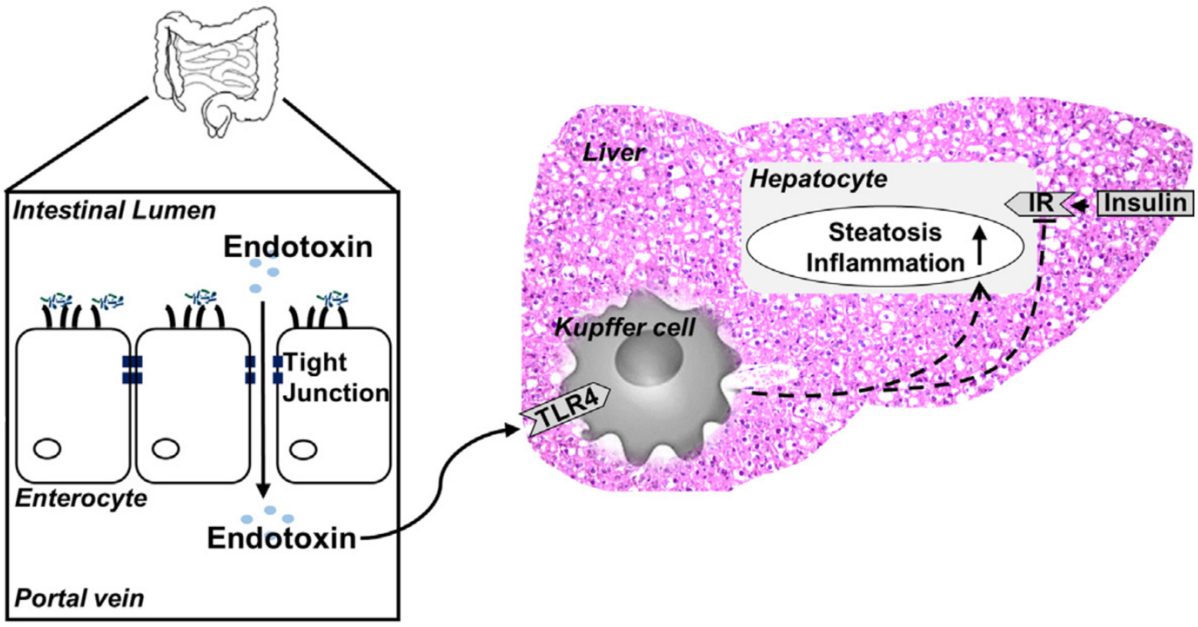

Figure 3: Molecular mechanism linking intestinal barrier dysfunction to the development of fatty liver *(for comparison, see ref. (56)). An elevated flux of gut-derived pro-inflammatory molecules, notably endotoxin, to the liver may activate hepatic Kupffer cells (54), resulting in an induction of the synthesis and secretion of pro-inflammatory cytokines, which, in turn, may dysregulate hepatic lipid and glucose metabolism, thus promoting ectopic lipid deposition and insulin resistance (53).* *Abbreviations: IR – insulin receptor, TLR4 – Toll-like receptor-4.*

1.3. *Caenorhabditis elegans* as a model for obesity and intestinal barrier dysfunction

Only recently, the potential of the nematode *Caenorhabditis elegans* (*C. elegans*) as a model organism in Food and Nutritional Science has been proposed (69,70). The *C. elegans* model provides many inherent advantages as a model organism including its small size, rapid lifecycle, sexual dimorphism, and large amount of progeny (for an overview, see ref. (71,72)). In addition, *C. elegans* ease of cultivation, low maintenance expenses, and lack of committee approval for experimentation can greatly reduce the time, costs, and potential ethical issues related to studies in higher animal models (for an overview, see ref. (70)).

C. elegans as a model for obesity

Mechanism involved in lipid synthesis, transport, storage, and breakdown are highly conserved between *C. elegans* and higher organism (73). In addition, many transcription factors, cellular energy sensors, endocrine, and neuronal regulators of fat metabolism are rather similar in mammalians and nematodes (see Figure 4B) (73,74).

Other than mammalians, *C. elegans* lacks dedicated adipocytes but stores major classes of lipids in the intestine, hypodermis, gonad, and eggs (75) (for an overview, see ref. (76)). The intestinal epithelial cells of *C. elegans* are considered the main site of lipid absorption, synthesis, storage, and mobilization (see Figure 4B) (for an overview, see ref. (76)). Based on its function in lipoprotein production and secretion, it has been hypothesized that the intestine of *C. elegans* carries out the functions of the human liver and intestine (77,78), whereas the skin-like hypodermis may function as a long-term energy storage site analogous to the human adipose tissue (78). Consistent with ectopic lipid deposition in the livers of insulin resistant mammalians, intestinal lipid deposits of *daf-2* insulin/IGF-1 receptor mutants were found to be enlarged (79), supporting the notion, that the intestine of *C. elegans* shares many characteristics with the human liver (77,78).

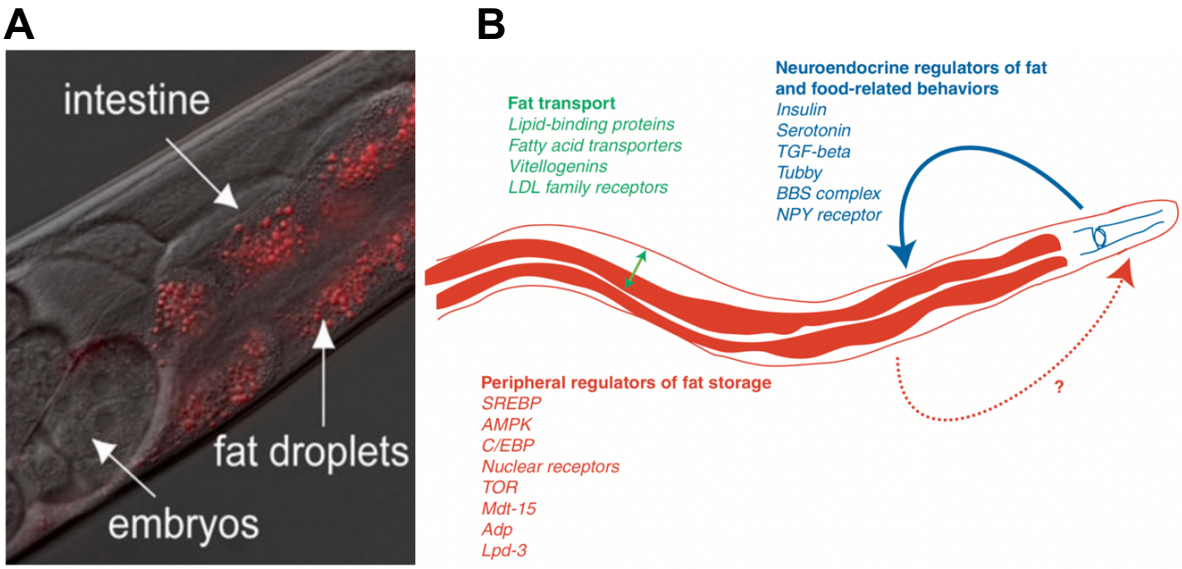

Figure 4: C. elegans as a model for obesity *(for an overview, see ref. (74,76)). (A) Lipid deposits in the intestine of C. elegans (76). (B) Lipid metabolic pathways conserved between C. elegans and humans (74). Abbreviations: AMPK – AMP-activated kinase, Adp – adipose, BSS – Bardet-Biedl syndrome, C/EBP – CCAAT/enhancer binding protein, LDL – low-density lipoprotein, Lpd-3 – lipid depleted-3, Mdt-15 – mediator-15, NPY – neuropeptide Y, SREBP – sterol regulatory element-binding protein, TGF-beta – transforming growth factor-beta, TOR – target of rapamycin.*

Depending on diet and developmental stage, 40 – 55 % of total extractable lipids from *C. elegans* constitute TG (for an overview, see ref. (76)). Notably, wildtype (WT) nematodes obtain the majority of FA for TG synthesis directly from bacterial diet, only 7 – 19 % of FA are derived from DNL (80,81). Studies further suggest that impaired insulin signaling is associated with an increase in DNL and elevated TG accumulation in *C. elegans* (81).

Similar like in mammalians, *C. elegans* TG and other neutral lipids are stored in lipid droplets (LD) (82). LD size is dynamic and intimately linked to lipid storage, mobilization, and catabolism (for an overview, see ref. (77)). Indeed, studies have shown that genetic and dietary factors can modulate LD expansion in *C. elegans* (83) e.g. Hellerer *et al.* reported that a shift in metabolism towards DNL is accompanied by an enlargement of LD in intestinal and hypodermal cells (84).

C. elegans as a model for intestinal barrier dysfunction

Figure 5A – C show the alimentary system of *C. elegans,* including the buccal cavity, pharynx, intestine, rectum, and annus (for an overview, see ref. (85)). The intestine of *C. elegans* is comprised of 20 large epithelial cells, which are arranged in bilateral symmetric pairs around a central lumen and carry a brush border (for an overview, see ref. (86)). Consistent with their proposed function in digestion and absorption, the intestinal epithelial cells of *C. elegans* secrete digestive enzymes and take up processed nutrients (for an overview, see ref. (86)).

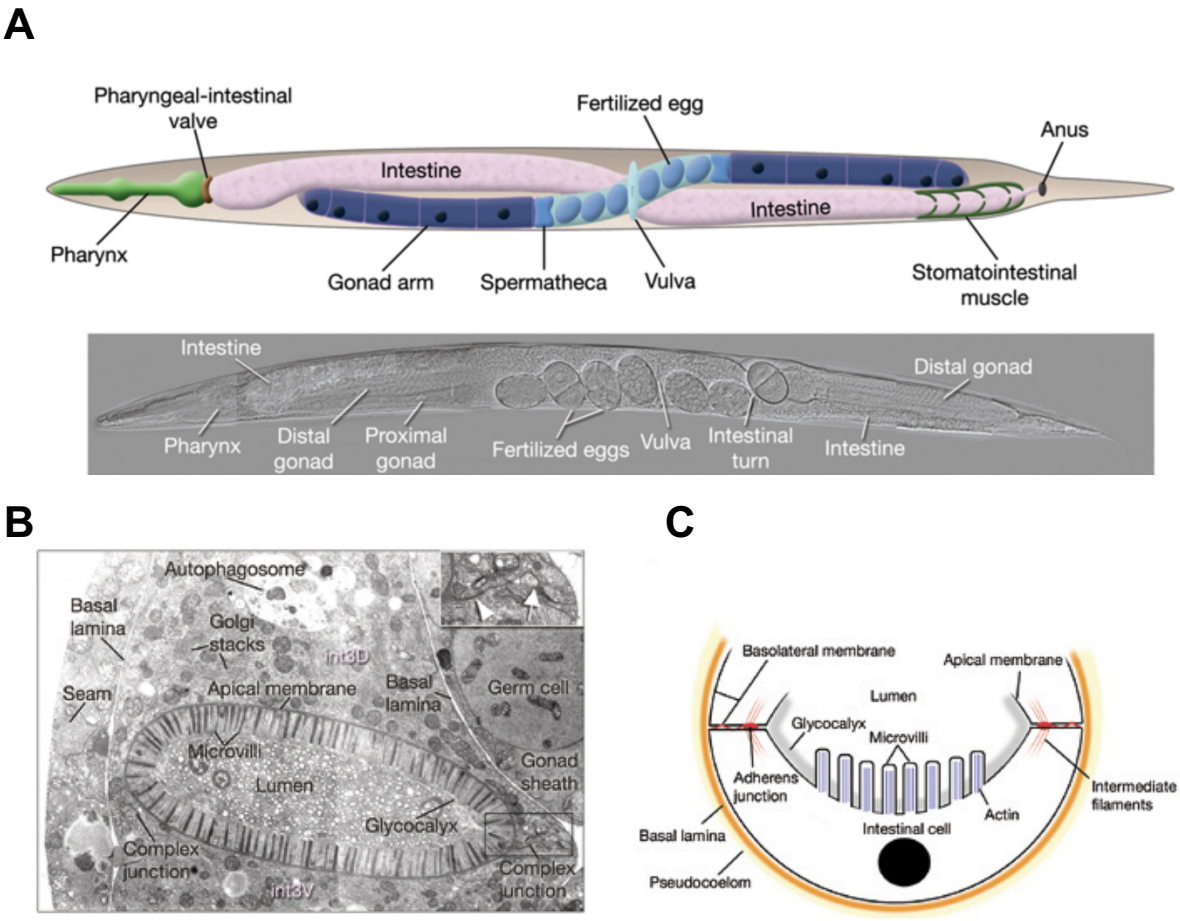

Figure 5: C. elegans as a model for intestinal barrier dysfunction *(for an overview, see ref. (85,86)).* ***(A)*** *Schematic representation and differential interference contrast microscopy image of the alimentary and reproductive system of C. elegans (85)* ***(B)*** *Transmission electron microscopy image and* ***(C)*** *diagram of a cross section through the intestinal epithelium (86).*

C. elegans lives on metabolically active bacteria (for an overview, see ref. (87)). Bacteria, which escape digestion, are assumed to colonize the intestinal lumen of *C. elegans* and exist as commensals or symbionts analogous to the gut microbiota in vertebrates (for an overview, see ref. (88)). Previous studies have shown that bacteria in the intestinal lumen can modulate *C. elegans* physiology independent of their role as a food source, supporting this notion (89,90).

Similar like in mammalians, the intestinal epithelium of *C. elegans* functions as a barrier against bacteria and bacterial toxins in the intestinal lumen (for an overview, see ref. (88)). However, in contrast to vertebrates, *C. elegans* does not bear typical TJs but instead harbors a single large apical junction, termed the *C. elegans* apical junction (CeAJ, see Figure 6), which has features of both, adherens junctions (AJs) and TJs (for an overview, see ref. (91)).

Claudins are proposed key regulators of TJ-permeability in vertebrates (for an overview, see ref. (92)). Studies have shown that claudin-deficient mice exhibit severe epithelial barrier defects, supporting this notion (93). Asano *et al.* (94) identified integral membrane proteins with sequence similarity to vertebral claudins in *C. elegans*. Furthermore, the authors documented an increase in paracellular permeability in the pharyngeal epithelium of CLC-1 deficient worms, suggesting an involvement of CLC-1 in the regulation of epithelial barrier function (94).

Zonula occludens (ZO) proteins are assumed to function as a scaffolding protein within vertebral TJs (95) (for an overview, see ref. (96)). Lockwood *et al.* (97) identified a single ortholog of the ZO family in *C. elegans*. Consistent with its proposed role in junctional anchorage to the cytoskeleton, loss of ZO ortholog 1 (ZOO-1) caused epithelial rupture during *C. elegans* morphogenesis (97).

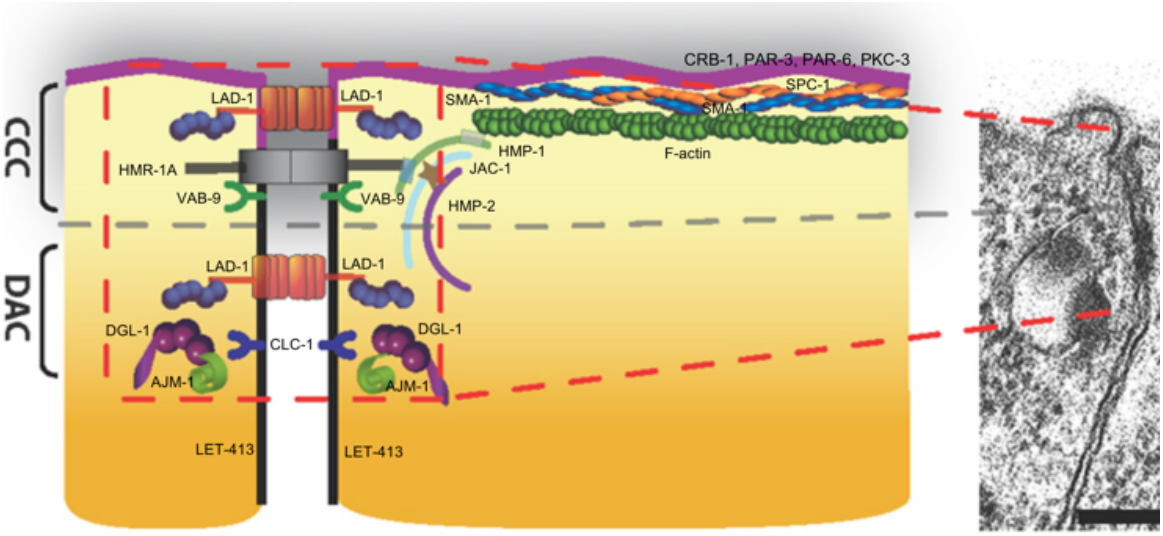

Figure 6: Structural organization of the C. elegans apical junction *(for an overview, see ref.* (91)*. The CeAJ contains at least two functionally distinct junctional complexes, the CCC and the DAC, which have features of both, AJs and TJs (91). Scale bar = 100 nm. Abbreviations: CeAJ – C. elegans apical junction, CCC – cadherin-catenin complex, DAC – DLG-1/AJM-1 complex.*

1.4. Aims

Lifestyle and especially dietary pattern have changed markedly throughout the last century, accompanied by a rise in the prevalence of obesity (98) and metabolic diseases (99), including NAFLD (100). As the ethology of many metabolic diseases yet remains to be fully elucidated, therapeutic options are still mainly focused on changes of lifestyle e.g. caloric restriction and physical activity (101). However, adherence is often poor, and relapse are high (102). Therefore, a better understanding of the molecular mechanism underlying the onset and progression of metabolic disease is desirable to improve disease prevention and therapy (53). Evidence from studies in rodent models of NAFLD indicates that diets high in sugar and herein particularly fructose can promote fat accumulation in the liver associated with a loss of TJ proteins in the upper parts of the small intestine and a concomitant increase in intestinal permeability (52,60,64,66,103). Starting from this background, the aim of the present study was to assess, if chronic intake of a diet high in fructose and glucose, respectively, also increases fat accumulation in *C. elegans* and if so, whether this is associated with a loss of proteins related to TJs in vertebrates.

2. Materials

2.1. *E. coli* culture

Organism

Escherichia coli OP50	Department of Pharmacognosy, University of Vienna

Media and buffer

LB agar

LB agar (Lennox)	CarlRoth GmbH & Co. KG, Karlsruhe
LB broth (Luria/Miller)	CarlRoth GmbH & Co. KG, Karlsruhe

DYT media

Tryptone/Peptone ex casein	CarlRoth GmbH & Co. KG, Karlsruhe
Yeast extract	AppliChem GmbH, Darmstadt
Sodium chloride (NaCl), ≥ 99 %	CarlRoth GmbH & Co. KG, Karlsruhe

Laboratory equipment

Petri dishes, with vents, Ø 90 mm	CarlRoth GmbH & Co. KG, Karlsruhe
Inoculation loops	Copan Diagnostics, Inc., Italy
Benchtop shaking incubator	Labwit Scientific Pty. Ltd., China
Gas burner	

2.2. *C. elegans* culture

Organism

Caenorhabditis elegans N2	Department of Pharmacognosy, University of Vienna

Media and buffer

NGM agar

Agar-Agar	CarlRoth GmbH & Co. KG, Karlsruhe
Tryptone/Peptone ex casein	CarlRoth GmbH & Co. KG, Karlsruhe
Sodium chloride (NaCl), ≥ 99 %	CarlRoth GmbH & Co. KG, Karlsruhe
Magnesium sulphate ($MgSO_4$), 99.5 %	Thermo Fisher GmbH, Karlsruhe
Calcium chloride dihydrate ($CaCl_2 \cdot 2H_2O$), ≥ 99 %	CarlRoth GmbH & Co. KG, Karlsruhe

Cholesterol in ethanol

Cholesterol ($C_{27}H_{46}O$)	CarlRoth GmbH & Co. KG, Karlsruhe
Ethanol (C_2H_6O), absolute	Merck KGaA, Darmstadt

Potassium phosphate buffer

Potassium dihydrogen phosphate (KH_2PO_4), ≥ 99 %	CarlRoth GmbH & Co. KG, Karlsruhe
Potassium phosphate dibasic trihydrate ($K_2HPO_4 \cdot 3H_2O$), high purity	VWR International GmbH, Darmstadt

Nystatin

Nystatin ($C_{47}H_{75}NO_{17}$)	Thermo Fisher GmbH, Karlsruhe
Ethanol (C_2H_6O), 96 %	Merck KGaA, Darmstadt
Ammonium acetate ($CH_3CO_2NH_4$)	AppliChem GmbH, Darmstadt

S buffer

Potassium dihydrogen phosphate (KH_2PO_4), ≥ 99 %	CarlRoth GmbH & Co. KG, Karlsruhe
Potassium phosphate dibasic trihydrate ($K_2HPO_4 \cdot 3H_2O$), high purity	VWR International GmbH, Darmstadt
Sodium chloride (NaCl), ≥ 99 %	CarlRoth GmbH & Co. KG, Karlsruhe

Sugar stock solutions

D-Fructose ($C_6H_{12}O_6$), > 99.5 %	CarlRoth GmbH & Co. KG, Karlsruhe
D-Glucose ($C_6H_{12}O_6$), ≥ 99.5 %	CarlRoth GmbH & Co. KG, Karlsruhe

Laboratory equipment

Stereomicroscope, Stemi 508	Carl Zeiss AG, Oberkochen, Germany
Platinum wire, 99.9 %, ∅ 0.25 mm	Stigma Aldrich Chemie GmbH, Steinheim
Cell scrapers, 28 cm	Greiner Bio-One GmbH, Frickenhausen
Omnifix® syringes, single-use	B/Braun, Meslungen, Germany
Rotilabo®-syringe filters, sterile	CarlRoth GmbH & Co. KG, Karlsruhe
Petri dishes, with vents, Ø 90 mm	CarlRoth GmbH & Co. KG, Karlsruhe
Cooled incubator, MIR-154	Panasonic Healthcare Co. Ltd., Japan
Microcentrifuge tubes, 1.7 ml	VWR International GmbH, Darmstadt
Pasteur pipettes, glass, 150 mm	Karl Hecht GmbH & Co. KG, Sondheim/Rhön, Germany

2.3. Lipid extraction and measurement of triglyceride concentration

Lipid extraction

Reagents

Chloroform ($CHCl_3$), ≥ 99.5 %	AppliChem GmbH, Darmstadt
Methanol (CH_4O), ≥ 99.9 %	CarlRoth GmbH & Co. KG, Karlsruhe
Albumin fraction V, powdered	CarlRoth GmbH & Co. KG, Karlsruhe

PBS

Sodium chloride (NaCl), ≥ 99 %	CarlRoth GmbH & Co. KG, Karlsruhe
Potassium chloride (KCl), ≥ 99.5 %	CarlRoth GmbH & Co. KG, Karlsruhe

Disodium hydrogen phosphate (Na_2HPO_4), ≥ 98 %	CarlRoth GmbH & Co. KG, Karlsruhe
Potassium phosphate dibasic trihydrate ($K_2HPO_4 \cdot 3H_2O$), high purity	VWR International GmbH, Darmstadt

Laboratory equipment

SONOPLUS sonotrode	Bandelin electronics, Berlin
SONOREX DIGITEC ultrasonic bath	Bandelin electronics, Berlin
Centrifugal vacuum concentrator	Eppendorf AG, Hamburg
Mixing block	Bioer Technology Co. Ltd., China

Triglyceride assay

Reagents

Triglyceride assay kit, TR210	Randox Laboratories Ltd., UK
Albumin fraction V, powdered	CarlRoth GmbH & Co. KG, Karlsruhe

Laboratory equipment

BRANDplates® microplates	BRAND GmbH & Co. KG, Wertheim
SpectraMax® M3 microplate reader	Molecular Devices LLC, San Jose, USA
SONOREX DIGITEC ultrasonic bath	Bandelin electronics, Berlin
Stainless steel water bath	Müller-Scherr Laborausrüstungs-gesellschaft GmbH & Co. KG, Linz

Bradford protein assay

Reagents

Protein Assay Dye Reagent Concentrate	Bio-Rad Laboratories Inc., Hercules, USA
Albumin fraction V, powdered	CarlRoth GmbH & Co. KG, Karlsruhe

Laboratory equipment

BRANDplates® microplates	BRAND GmbH & Co. KG, Wertheim
SpectraMax® M3 microplate reader	Molecular Devices LLC, San Jose, USA

2.4. Oil Red O staining

Reagents

Oil Red O	Stigma Aldrich Chemie GmbH, Steinheim
Isopropanol (C_3H_8O), ≥ 99.5 %	CarlRoth GmbH & Co. KG, Karlsruhe
Triton X-100	CarlRoth GmbH & Co. KG, Karlsruhe

M9 buffer

Potassium dihydrogen phosphate (KH_2PO_4), ≥ 99 %	CarlRoth GmbH & Co. KG, Karlsruhe
Sodium chloride (NaCl), ≥ 99 %	CarlRoth GmbH & Co. KG, Karlsruhe
Disodium hydrogen phosphate (Na_2HPO_4), ≥ 98 %	CarlRoth GmbH & Co. KG, Karlsruhe
Magnesium sulphate ($MgSO_4$), 99.5 %	Thermo Fisher GmbH, Karlsruhe

Agarose pads

GOLD Universal Agarose	Budenheim, Germany

Laboratory equipment

Benchtop shaking incubator	Labwit Scientific Pty. Ltd., China
Omnifix® syringes, single use	B/Braun, Meslungen, Germany
Rotilabo® syringe filters, sterile	CarlRoth GmbH & Co. KG, Karlsruhe
Mixing block	Bioer Technology Co. Ltd., China
Leica DM6 B upright microscope	Leica Microsystems CMS GmbH, Wetzlar

Cover slips	CarlRoth GmbH & Co. KG, Karlsruhe
Standard microscope slides	CarlRoth GmbH & Co. KG, Karlsruhe

2.5. Intestinal barrier function assay

Reagents

Erioglaucine disodium salt, pure	VWR International GmbH, Darmstadt
Sodium azide (NaN_3), 99 %	VWR International GmbH, Darmstadt

M9 buffer

Potassium dihydrogen phosphate (KH_2PO_4), ≥ 99 %	CarlRoth GmbH & Co. KG, Karlsruhe
Sodium chloride (NaCl), ≥ 99 %	CarlRoth GmbH & Co. KG, Karlsruhe
Disodium hydrogen phosphate (Na_2HPO_4), ≥ 98 %	CarlRoth GmbH & Co. KG, Karlsruhe
Magnesium sulphate ($MgSO_4$), 99.5 %	Thermo Fisher GmbH, Karlsruhe

S media

Magnesium sulphate ($MgSO_4$), 99.5 %	Thermo Fisher GmbH, Karlsruhe
Calcium chloride dihydrate ($CaCl_2 \cdot 2H_2O$), ≥ 99 %	CarlRoth GmbH & Co. KG, Karlsruhe

Cholesterol in ethanol

Cholesterol ($C_{27}H_{46}O$)	CarlRoth GmbH & Co. KG, Karlsruhe
Ethanol (C_2H_6O), absolute	Merck KGaA, Darmstadt

Potassium Citrate

Citric acid monohydrate ($C_6H_8O_7•H_2O$), ≥ 99.0 %	Stigma Aldrich Chemie GmbH, Steinheim
Potassium citrate tribasic monohydrate ($C_6H_5K_3O_7•H_2O$), ≥ 99.0 %	Stigma Aldrich Chemie GmbH, Steinheim

Trace metal solution

Disodium EDTA	VWR International GmbH, Darmstadt
Iron (II) sulfate heptahydrate ($FeSO_4•7H_2O$)	VWR International GmbH, Darmstadt
Manganese (II) chloride tetrahydrate ($MnCl_2•4H_2O$)	VWR International GmbH, Darmstadt
Copper (II) sulfate pentahydrate ($CuSO_4•5H_2O$)	VWR International GmbH, Darmstadt
Zinc sulfate heptahydrate ($ZnSO_4•4H_2O$)	Stigma Aldrich Chemie GmbH, Steinheim

S basal

Sodium chloride (NaCl), ≥ 99 %	CarlRoth GmbH & Co. KG, Karlsruhe
Potassium dihydrogen phosphate (KH_2PO_4), ≥ 99 %	CarlRoth GmbH & Co. KG, Karlsruhe
Potassium phosphate dibasic trihydrate ($K_2HPO_4•3H_2O$), high purity	VWR International GmbH, Darmstadt

Laboratory equipment

TC plate, 12 well, standard, F	Sarstedt AG & Co. KG, Nümbrecht
Platinum wire, 99.9 %, ∅ 0.25 mm	Stigma Aldrich Chemie GmbH, Steinheim
Cover slips	CarlRoth GmbH & Co. KG, Karlsruhe
Standard microscope slides	CarlRoth GmbH & Co. KG, Karlsruhe
Stereomicroscope, Stemi 508	Carl Zeiss AG, Oberkochen, Germany
Leica DM6 B upright microscope	Leica Microsystems CMS GmbH, Wetzlar

2.6. RNA isolation and quantitative mRNA expression analysis

RNA isolation

Reagents

peqGOLD TriFast™	VWR International GmbH, Darmstadt
Chloroform ($CHCl_3$), ≥ 99.5 %	AppliChem GmbH, Darmstadt
Isopropanol (C_3H_8O), ≥ 99.5 %	CarlRoth GmbH & Co. KG, Karlsruhe
Ethanol (C_2H_6O), absolute	Merck KGaA, Darmstadt
ROTIPURAN® water	CarlRoth GmbH & Co. KG, Karlsruhe

Laboratory equipment

TissueLyser II bead mill	Qiagen GmbH, Hilden, Germany
TissueLyser adapter set, 2 x 24	Qiagen GmbH, Hilden, Germany
Glass beads, 1 mm	CarlRoth GmbH & Co. KG, Karlsruhe
Mixing block	Bioer Technology Co. Ltd., China

RNA concentration measurement and quality control

Reagents

Nuclease-free water	Promega Cooperation, Madison, USA
GOLD Universal Agarose	Budenheim, Germany
DNA-Dye NonTox	AppliChem GmbH, Darmstadt

TBE buffer

TRIS ($C_4H_{11}NO_3$)	CarlRoth GmbH & Co. KG, Karlsruhe
Boric acid (H_3PO_3), ≥ 99.5 %	CarlRoth GmbH & Co. KG, Karlsruhe
EDTA ($C_{10}H_{16}N_2O_8$), ≥ 99 %	CarlRoth GmbH & Co. KG, Karlsruhe

Laboratory equipment

UV-Star® 96-well plate	Greiner Bio-One GmbH, Frickenhausen
SpectraMax® M3 microplate reader	Molecular Devices LLC, San Jose, USA

Horizontal gel system	Cleaver Scientific Ltd., Warwickshire, UK
Casting dams and combs	Cleaver Scientific Ltd., Warwickshire, UK
High-current power supply	Bio-Rad Laboratories Inc, Hercules, USA
Gel imaging system	Bio-Rad Laboratories Inc, Hercules, USA

cDNA synthesis

Reagents

RQ1 RNase-Free DNase	Promega Cooperation, Madison, USA
RQ1 DNase 10X Reaction Buffer	Promega Cooperation, Madison, USA
Stop Solution	Promega Cooperation, Madison, USA
Reverse Transcription System	Promega Cooperation, Madison, USA
Nuclease-free water	Promega Cooperation, Madison, USA

Laboratory equipment

Multiply® -μStrip Pro 8-strip, 0.2 μl	Sarstedt AG & Co. KG, Nümbrecht
LifeECO Thermal cycler	Bioer Technology Co Ltd, China

RT-qPCR

Reagents

iTaq™ Universal SYBR® Green Supermix	Bio-Rad Laboratories Inc, Hercules, USA
Nuclease-free water	Promega Cooperation, Madison, USA

Primer

cdc-42	Eurofins Genomics, Ebersberg, Germany
clc-1	Eurofins Genomics, Ebersberg, Germany
zoo-1	Eurofins Genomics, Ebersberg, Germany

Laboratory equipment

Hard-Shell® 96-well PCR plates	Bio-Rad Laboratories Inc., Hercules, USA
CFX Connect™ Real-Time system	Bio-Rad Laboratories Inc., Hercules, USA

2.7. General laboratory equipment

Tabletop centrifuge, Z 216 MK	Hermle Labortechnik GmbH, Wehingen
Tabletop centrifuge, Z 446 K	Hermle Labortechnik GmbH, Wehingen
Palm microcentrifuge, D1008	DLAB Scientific Inc., Agoura Hills, USA
Vortex mixer, REAX 2000	Heidolph GmbH & Co. KG, Schwabach
Analytical balance	Sartorius Stedim Plastics GmbH
Weighing dishes	CarlRoth GmbH & Co. KG, Karlsruhe
Magnetic stirrer with heating function	Phoenix Instrument, Grabsen, Germany
Rotilabo® Economy magnetic bars	CarlRoth GmbH & Co. KG, Karlsruhe
Eppendorf Research ® plus pipettes	Eppendorf AG, Hamburg
Pipetting tips	Sarstedt AG & Co. KG, Nümbrecht
Serological pipettes	Sarstedt AG & Co. KG, Nümbrecht
LEVO pipette controller	DLAB Scientific Inc., Agoura Hills, USA
SafeSeal reaction tubes	Sarstedt AG & Co. KG, Nümbrecht
Screw-cap tubes, 15 ml, 50 ml	Sarstedt AG & Co. KG, Nümbrecht
BRAND® PARAFILM® M Sealing film	BRAND GmbH & Co. KG, Wertheim
KGW Isotherm™ Dewar flask	Fisher Scientific GmbH, Schwerte

2.8. Software

Graph Pad Prism	GraphPad Prism Inc., San Diego, USA
Image Lab	Bio-Rad Laboratories Inc., Hercules, USA
ImageJ	National Institute of Health, Bethesda, USA
LAS X	Leica Microsystems CMS GmbH, Wetzlar
CFX Manager	Bio-Rad Laboratories Inc., Hercules, USA

3. Methods

3.1. Worm culturing

Maintenance of C. elegans

WT *C. elegans* strain N2 (Bristol) was maintained on 9 cm-diameter nematode growth media (NGM) plates in a 20 °C temperature-controlled incubator as described by Stiernagle (87). Nematodes were grown in monoxenic culture with non-pathogenic *Escherichia coli* (*E. coli)* strain OP50 (104). NGM plates for experiments were seeded with 500 µl of 2X *E. coli* OP50 suspension and incubated at 20 °C the evening prior to use (105). For the preparation of bacterial food source an overnight culture of *E. coli* OP50 was streaked on LB agar and incubated for 2 days at 20 °C (87). A single colony, isolated from a LB streak plate, was subsequently used to inoculate 100 ml of DYT media. The inoculated growth media was incubated overnight at 37 °C while rocking at 100 rcf and subsequently double-concentrated by centrifugation for 30 min at 3,220 rcf and 4 °C. 2X *E. coli* OP50 suspensions were stored at 4 °C until later use.

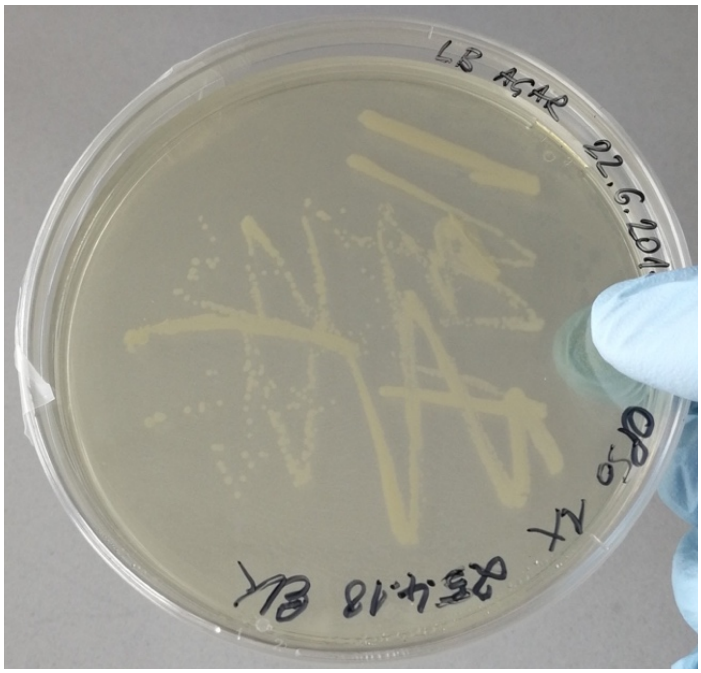

Figure 7: Representative picture of a LB streak plate.

Synchronization of nematodes

Figure 8 depictures the lifecycle of *C. elegans* (106). To obtain an age-synchronized nematode population, adult hermaphrodites were allowed to replicate until their progeny reached the L4 stage. L4-stage larvae were incubated for 4 days at 20 °C (107). Subsequently, adult worms were washed off plates with sterile water and eggs were loosened using a cell scraper. The suspension, containing eggs and bacteria, was transferred into a 15-ml falcon tube and pelleted by 1-min centrifugation at 200 rcf. Subsequently, the supernatant was removed, and eggs were rinsed with sterile water. Finally, eggs were resuspended in 1 ml of sterile water and 50 µl of the suspension was spotted on regular NGM plates, which were incubated overnight at 20 °C. The following day, nematodes bigger than newly hatched larvae were removed using a worm picker.

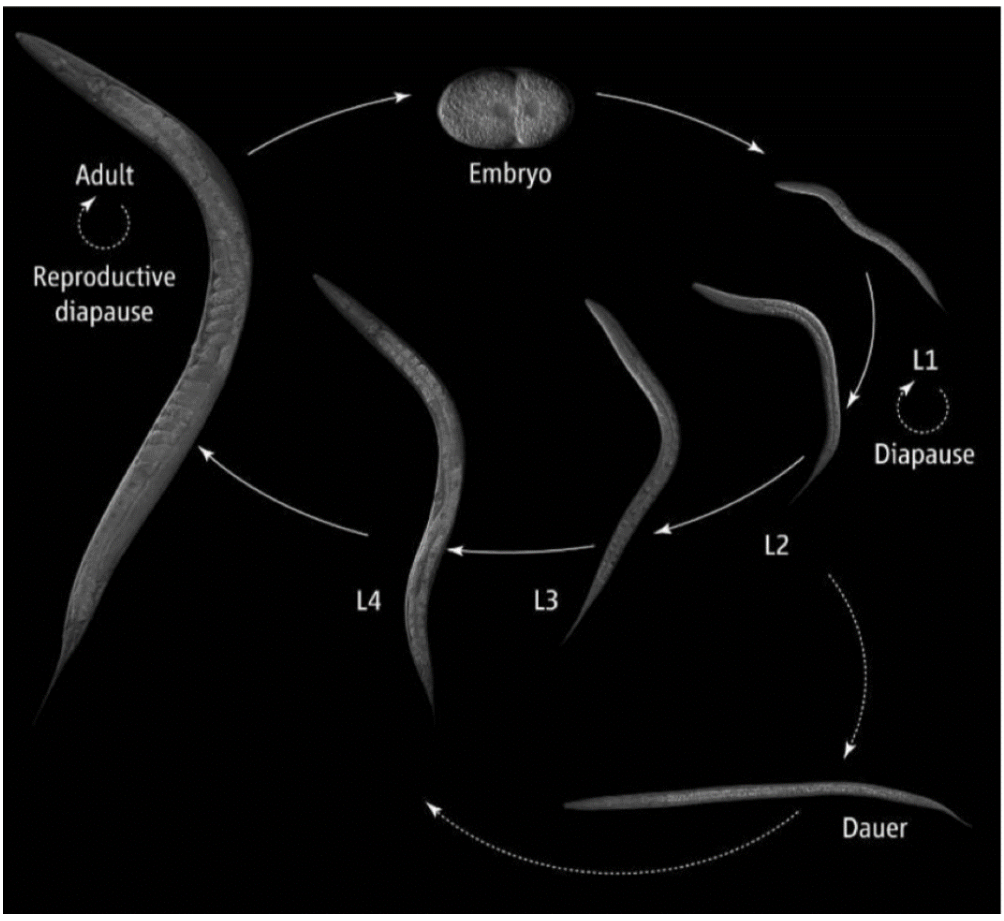

Figure 8: Schematic drawing of C. elegans life cycle (106). *L4-stage larvae are characterized by a half circle in the body midsection which will eventually develop into the vulva (107).*

Exposure of nematodes to monosaccharides

To investigate the effects of chronic exposure to monosaccharides on fat storage and intestinal barrier function in the *C. elegans* model, young adult (YA) worms were cultured on NGM plates with 25 mM and 50 mM of fructose and glucose, respectively, for a total of 4 days. All plates were prepared from the same batch of NGM agar as detailed in the annex.

Figure 9 gives an overview of the experimental setup of the *C. elegans* trials conducted. The number of plates and animals per plate is given in Supplementary Table 1 (see annex). On the first day of adulthood, age-synchronized nematodes were transferred into a 15 ml-falcon tube using S buffer and pelleted by 1-min centrifugation at 200 rcf. Subsequently, the supernatant was aspirated, and worms were rinsed with S buffer. After nematodes settled again by gravity, the supernatant was discarded, and 2 ml of S buffer added. Finally, 50 µl of the suspension, containing 100 – 150 worms, were spotted on NGM plates with added monosaccharides.

The intervention lasted for a total of 4 days during which nematodes were transferred at 24-h intervals. To this end, worms receiving the same treatments were collected in the same falcon tube, pelleted by 1-min centrifugation, and rinsed with S buffer. After settling again by gravity, nematodes were resuspended in S buffer, and 150 µl of the suspension were spotted on NGM plates with added monosaccharides.

Harvesting of nematodes

After the respective incubation period, nematodes were harvested with ice-cold S buffer and rinsed by 1-min centrifugation at 200 rcf and 4 °C. Subsequently, nematodes were aliquoted into ice-cold polypropylene tubes and pelleted at 2,000 rcf and 4 °C. Then, the buffer was aspirated completely, and worms were prep frozen in liquid nitrogen. Frozen worm pellets were stored at – 80 °C until later processing.

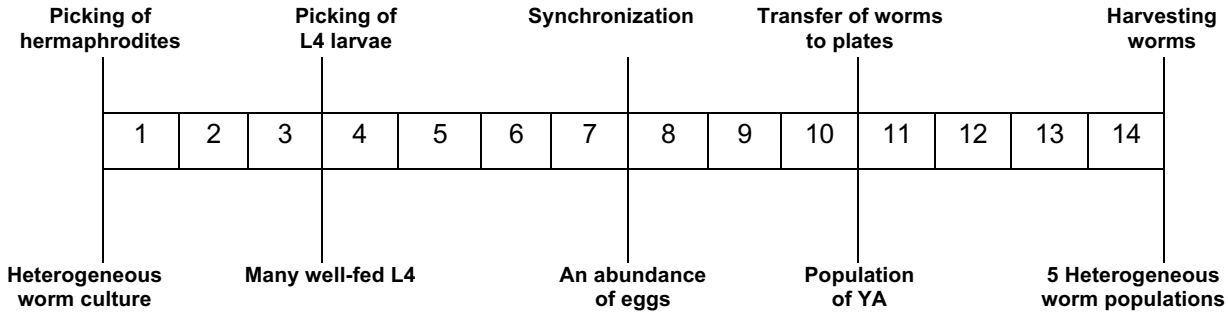

Figure 9: Experimental setup of the C. elegans trails.

3.2. Biochemical assessment of *C. elegans* fat mass

Extraction and purification of lipids from worm homogenates

Lipids were extracted using the method first described by Folch *et al.* (108). In brief, frozen worm pellets were homogenized with 2X PBS by ultrasound (2 x 20 sec, 10 % power). Then, one part of the homogenate was diluted to a final volume of 500 µl and heated for 5 min at 80 °C. 500-µl aliquots were cooled to RT and subsequently homogenized with 250 µl methanol and 500 µl chloroform, again using ultrasound. The crude extract was incubated for 2 h at RT and subsequently centrifuged for 5 min at maximum speed and 4 °C. Then, 400 µl of the lower chloroform phase, containing lipids, were transferred into a new reaction tube and evaporated in a centrifugal vacuum concentrator for 10 – 20 min (depending on pellet volume). The lipid residue was resuspended in 5 % BSA and solubilized by heating (1 h, 55 °C) and sonification (2 x 20 sec, 10 % power). Lipid extracts were frozen overnight at – 80 °C. The following day, extracts were reheated (10 min, 55 °C) and resolved by ultrasound (2 x 20 sec, 10 % power). Subsequently, samples were heated again for 1 h at 55 °C and finally frozen at – 80 °C.

Measurement of triglyceride concentration in lipid extracts

The frozen samples were reheated in a 37 °C water bath for 2 h and resolved by ultrasound. Subsequently, TG concentration in lipid extracts was determined spectrophotometrically using an enzymatic assay kit purchased from RANDOX laboratories. Figure 10 outlines the principle of the GPO-POD method, which constitutes the basis of the assay (109).

	LPL	
TG	→	Glycerol + FFA
	GK	
Glycerol + ATP	→	G3P + ADP
	GPO	
G3P + O_2	→	DHAP + H_2O_2
	POD	
$2H_2O_2$ + 4-AP + Chlorophenol	→	Quinonimine dye + HCl + $4H_2O$

Figure 10: Principle of the GPO-POD *(for an overview, see ref. (109)). The GPO-POD method links the colorimetric detection of H_2O_2, generated during the oxidation of G3P by GPO, to the hydrolysis of TG by LPL. H_2O_2 constitutes a substrate for POD, which catalyzes the formation of a red chromogen with an absorption maximum at 505 nm from 4-AP and chlorophenol (109). Abbreviations: ADP – adenosine diphosphate, ATP – adenosine triphosphate, 4-AP – 4-aminophenazone, DHAP – dihydroxy acetone phosphate, FFA – free fatty acids, GK – glycerol kinase, G3P – glycerol-3-phosphate, GPO – glycerol-3-phosphat oxidase, LPL – lipoprotein lipase, POD – peroxidase, TG – triglycerides.*

The TG assay was carried out in a microplate reader in triplicates. In brief, 2 µl of samples, TG standard (190 mg/dl), and blank (5 % BSA) were mixed with 200 µl of the enzymatic reagent in a 96-well plate. After 10 min incubation at 37 °C, absorbance was determined by a spectrophotometric reading at 500 nm and TG concentration in lipid extracts was calculated as follows:

$$\text{Triglycerides (mg/dl)} = \frac{(\text{Absorbance}_{\text{Sample}} - \text{Absorbance}_{\text{Blank}}) \times \text{Concentration}_{\text{Standard}}}{(\text{Absorbance}_{\text{Standard}} - \text{Absorbance}_{\text{Blank}}) \times \text{Dilution factor}_{5\%\text{BSA}}}$$

Subsequently, TG concentration in lipid extracts was normalized to protein concentration in worm homogenates.

Measurement of protein concentration in worm homogenates

Protein concentration in worm homogenates was determined using a commercially available kit (Bio-Rad protein assay) based on the method of Bradford (110). The latter links the interaction of Coomassie Brilliant Blue G-250 with basic and aromatic amino acid residues in proteins to an increase in absorption at 595 nm (110,111).

Table 1: Preparation of the Bradford standard series.

Standard	**2X PBS (µl)[1]**	**Serial dilutions**	**BSA (µg/µl)**
A	198	+ 2 µl BSA stock (100 mg/ml)	1.0
B	100	+ 100 µl Standard A	0.5
C	100	+ 100 µl Standard B	0.25
D	100	+ 100 µl Standard C	0.125
E	100	+ 100 µl Standard D	0.0625
F	100	+ 100 µl Standard F	0.0

[1] diluted 1:3 or 1:10 in ddH_2O

The assay was carried out in a microplate reader in triplicates using a serial dilution series of BSA in 2X PBS (see Table 1) as a standard. In brief, worm homogenates were centrifuged for 5 min at maximum speed to remove any insoluble material. The supernatant was transferred into a reaction tube and diluted in distilled, deionized water (ddH_2O). Subsequently, 5 µl of samples, standards and blank (diluted extraction buffer), respectively, were mixed with 200 µl of dye reagent in a 96-well plate. After 10 min incubation at RT, absorbance was determined by a spectrophotometric reading at

595 nm and protein concentration in worm homogenates was calculated as follows using a standard curve (for comparison, see Figure 10):

$$y = k \times x + d$$

$$\text{Protein } (\mu g/\mu l) = \frac{\left(\text{Mean Absorbance}_{\text{Sample}} - \text{Mean Absorbance}_{\text{Blank}}\right) \times \text{Dilution factor}_{\text{ddH2O}}}{\text{k} \times \text{Dilution factor}_{\text{2XPBS}}}$$

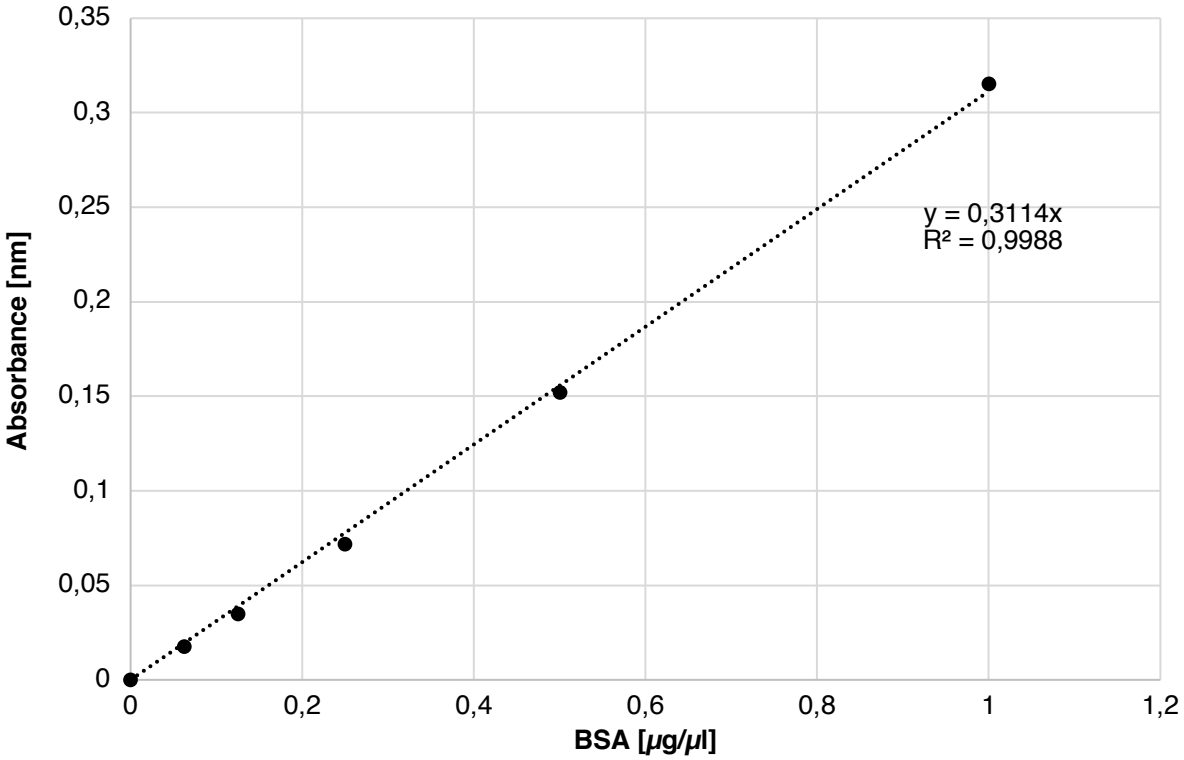

Figure 11: Exemplary Bradford standard curve. *Shown is the mean absorption of the protein standards plotted against their BSA concentration. Abbreviations: BSA – bovine serum albumin.*

3.3. Visualization of *C. elegans* fat stores

Fixative-based Oil Red O staining

Oil Red O (ORO) staining was carried out using the protocol of O'Rourke *et al.* (75) with minor modifications as described by Heestand *et al.* (112). For the staining, ORO stock solution was freshly diluted to 60 % ORO working solution and stirred for several hours at RT. After the respective incubation period, 200 – 300 nematodes per treatment were transferred into a 15-ml falcon tube using M9 buffer and allowed to settle by gravity. Subsequently, the supernatant was discarded, and worms were rinsed with M9 buffer. Then, nematodes were aliquoted into polypropylene tubes and allowed to settle again by gravity. Subsequently, the buffer was removed and 240 µl of 50 % isopropanol added to the nematodes, which were then fixed for 15 min while rocking at 300 rcf. Then, the fixative was removed and 1 ml of freshly filtered ORO working solution added. Nematodes were soaked in ORO stain overnight while rocking at 500 rcf. Subsequently, the dye was removed, and worms were rinsed with 1 ml of 1X PBS. After nematodes settled again by gravity, the supernatant was aspirated, and nematodes were resuspended in 200 µl of 1X PBS 0.01 % Triton X-100. Finally, 30 µl of the suspension, containing 10 – 30 worms, were mounted on a glass slide with an 5 % agarose pad and imaged at 400 × magnification using a Leica camera microscope.

Image-based quantification of Oil Red O staining

For quantification of ORO staining the protocol of Wählby *et al.* (113) was adapted. Using the image processing and analysis platform ImageJ, the original RGB images were inverted and split into their respective color channels. Regions corresponding to worms were subsequently identified in the blue image channel, while ORO-stained areas were identified in the green image channel (114). After worms and stained areas were separated from the image background by manual thresholding, size and intensity measurements were obtained from the individual worms by using the analyze particles function of ImageJ. The size of the stained areas was then related to the size of the

nematodes to obtain an estimate for the mean fat content per worm. Larvae and gravid hermaphrodites were excluded from the image analysis (69).

3.4. Assessment of *C. elegans* intestinal barrier function

Intestinal barrier function was assessed using a non-invasive dye-leakage assay, developed by Gelino *et al.* (115) based on the 'Smurf' assay first described by Rera *et al*. (116,117). In brief, 100 nematodes per treatment were submerged in liquid bacterial culture mixed with non-absorbable blue food dye (1 % w/v erioglaucine disodium salt, see annex). After 1, 3, and 6 h of incubation at 20 °C, 10 worms per treatment were transferred on a glass slide with an agarose pad, immobilized by treatment with 30 µl of 25 mM sodium azide (NaN_3) in M9 buffer, and examined for intestinal dye-leakage into the body cavity using a Leica camera microscope at 100 × magnification.

3.5. Analysis of mRNA expression of *C. elegans* apical junction proteins

Isolation of total RNA from worms

Total RNA from worms was isolated using a commercially available kit for RNA isolation based on the method of Chomczynski and Sacchi (118). In brief, 1 ml of Trizol and 30 mg of 1 mm glass beads were added to the frozen worm pellets which were then homogenized 3 x 1 min at 30 Hz in a precooled bead mill. The resulting homogenate was incubated for 5 min while rocking at 300 rcf and subsequently incubated for 5 min at RT. Then, 200 µl of chloroform was added to the samples which were then homogenized for 15 sec at 25 Hz. The resulting homogenate was incubated for 3 min on ice and subsequently centrifuged for 20 min at 12,000 rcf and 4 °C to separate total RNA from DNA and proteins. The top aqueous phase, containing RNA, was then mixed with 1.1 times the volume of isopropanol and incubated for 10 min on ice to precipitate RNA. Subsequently, samples were centrifuged again for 20 min at

12,000 rcf and 4 °C, the supernatant was discarded, and the RNA, visible as a gel like pellet at the bottom of the tube, was rinsed with 1 ml of 80 % ethanol. After 10 min centrifugation at 7,500 rcf, the supernatant was removed completely, and RNA pellets were air-dried for 10 min. Then, the RNA was resuspended in 10 or 40 µl of nuclease-free water (depending on pellet volume), solubilized by heating at 65 °C for 5 min, and finally frozen at – 80 °C.

Assessment of RNA integrity, concentration, and purity

To assure total integrity of extracted RNA, an agarose gel electrophoresis was performed. In short, 0.8 µl of the RNA samples were diluted in 5 µl of ddH_2O and resuspended in 0.8 µl of non-toxic DNA dye. Samples were loaded on an agarose gel in 1X TBE buffer and electrophoresed at 100 Volts for 40 min. Subsequently, the agarose gel was transferred into a detection chamber equipped with an UV light source to visualize RNA fragments. Figure 12 shows a gel electrophoresis of RNA extracted from *C. elegans*. In general, high quality RNA exhibits a typical electrophoresis pattern characterized by two prominent bands representing the 28S and 18S ribosomal RNAs and one faint band corresponding to the 5S rRNA (118).

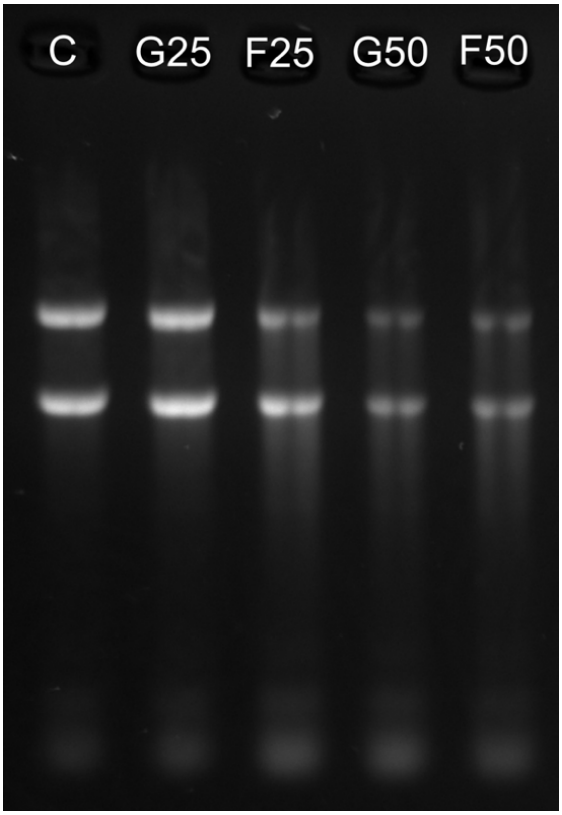

Figure 12: Representative picture of a gel electrophoresis of RNA isolated from C. elegans. *Abbreviations: C – control, G25 – 25 mM glucose, F25 – 25 mM fructose, G50 – 50 mM glucose, F50 – 50 mM fructose.*

Assessment of total RNA concentration and purity was carried out in a microplate reader. In brief, 2 μl of RNA samples were diluted with 98 μl of nuclease-free water (NFW) in an UV-transparent microplate and measurements were carried out at 260, 280, and 230 nm (118). Measurements at 260 nm were subsequently used to calculate RNA concentration with the formula first described by Chomczynski and Sacchi (118). Furthermore, 260/280 and 260/230 ratios of absorbance were determined to assess if samples were contaminated with protein or DNA (118). Absorbance pattern of pure preparations of nucleic acids are shown in Table 2 (for an overview, see ref. (119)). Only samples with a 260/280 ratio of absorbance > 1.8 were used for further measurements.

Table 2: Absorbance of pure preparations of nucleic acids (119).

$A_{260/280}$	DNA ~ 1.6 RNA ~ 2.0
$A_{260/230}$	1.8 – 2.2

Reverse transcription of RNA to complementary DNA

Prior to further processing, a mixture of 1.11 μg RNA in 8 μl of NFW was incubated with 1 μl of DNAse I and 1 μl of DNase 10X reaction buffer (400 mM Tris-HCl, 100 mM $MgSO_4$, 10 mM $CaCl_2$) to remove DNA contaminations. DNA digestion was carried out in a thermal cycler at 37 °C for 30 min. The reaction was terminated by the addition of 1 μl stop solution (20 mM EGTA) and 10 minutes incubation at 65 °C. After 1-min incubation on ice, reverse transcription of total RNA to complementary DNA (cDNA) was accomplished with a ready-to-use kit purchased from Promega cooperation. Following the instructions of the manufacturer, samples were incubated with 20 µl reaction mix and cDNA synthesis was carried out in a thermal cycler as detailed in Table 3 and 4, respectively. Subsequently, samples were diluted with 80 µl of NFW and stored at – 20 °C until further use.

Table 3: cDNA synthesis reaction mix.

Reagents	**µl/sample**
25mM $MgCl_2$	4
Reverse transcription buffer	2
10mM dNTP mixture	2
Recombinant RNAsin® ribonuclease inhibitor	0.5
Random primers	1
AMV reverse transcriptase	0.6

Table 4: cDNA synthesis parameters.

Temperature (°C)	**Time (min)**
25	10
42	15
95	15
4	5

Assessment of mRNA expression by RT-qPCR

Real-time quantitative polymerase chain reaction (RT-qPCR) was performed using a ready-made master mix containing iTaq DNA polymerase, dNTPs, $MgCl_2$, and the DNA-binding fluorophore SYBR® Green I. For the reaction mix, 3 µl of DEPC-treated water, 1 µl of gene-specific forward as well as reverse primers (see Table 5) and 5 µl of cDNA template or non-template control (DEPC-treated water) were added to 10 µl master mix on ice.

Table 5: Primer sequence information.

	***forward* (5´ → 3´)**	***reverse* (5´ → 3´)**
cdc-42	AGC CAT TCT GGC CGC TCT CG	GCA ACC GCT TCT CGT TTG GC
clc-1	CCG CCG CAG ATA AGA TGA GG	TTT GAC ATG CCT TGC CTG CT
zoo-1	ATT TTC TGC GCC TCG TGC AT	GGC CGT TAC CAC CCA CTG AC

Amplifications were carried out in a RT-qPCR detection system as detailed in Table 6. In brief, each RT-qPCR was primed by an initial DNA denaturation step, followed by several cycles of combined amplification and detection at primer-specific temperatures, and a final melt curve analysis.

Table 6: Thermal cycling protocols.

	Temp. (°C)	**Time (sec)**	**Cycles (n)**
Polymerase activation DNA denaturation	95	30	
DNA denaturation	95	5	45 (*cdc-42*) 50 (*clc-1*) 42 (*zoo-1*)
Annealing/elongation Plate read	60	30	
	95	10	
Melt curve analysis	65 – 95	5	

Figure 13A shows a plot of data generated by RT-qPCR using SYBR® Green I detection after each PCR cycle (for comparison, see ref. (120)). During the exponential phase of the PCR, the fluorescent signal emitted by SYBR® Green I, when bound to the amplicon of the target sequence, is assumed to be directly proportional to the initial number of target transcripts in the sample (120,121). The number of PCR cycles, at which the fluorescence signal for the target transcripts (*zoo-1, clc-1*) crossed a threshold defined as C_t, was subsequently related to a reference transcript (*cdc-42*) and a calibrator (study-specific control) using the $2^{-\Delta\Delta Ct}$ method (for an overview, see ref. (121)) as described below.

$$\Delta C_t = C_{t\,target} - C_{t\,reference}$$

$$\Delta\Delta C_t = \Delta C_{t\,calibrator} - \Delta C_{t\,sample}$$

$$\text{mRNA expression (fold change)} = 2^{\Delta\Delta C_t}$$

To assure the presence of a single PCR product, samples were subjected to a melt curve analysis following the final cycle of the PCR (see Figure 13B).

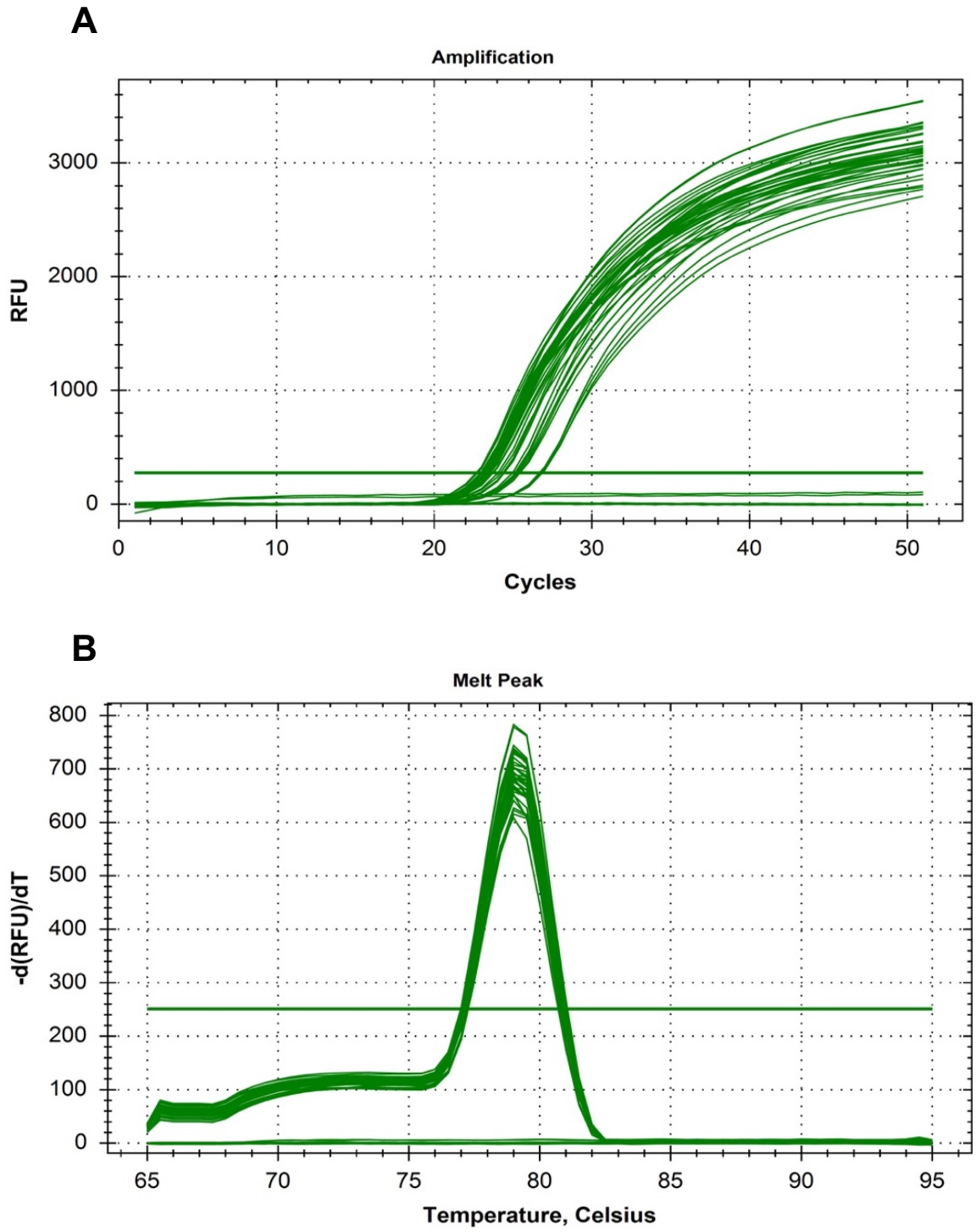

Figure 13: RT-qPCR of clc-1 mRNA expression in C. elegans. *(A) Plot of ∆ RFU versus PCR cycle number obtained from SYBR ® Green I detection of clc-1 mRNA. The presence of a single melt peak in plot (B) verified the detection of no other PCR product than the amplicon of the target sequence (see ref. (120) for comparison).*

3.6. Statistical analysis

All data were analyzed using GraphPad Prism 7 (GraphPad Prism Inc., San Diego, USA). Results are presented as mean percentage of control ± standard error of mean (SEM). Outliners identified by the Grubbs' test were excluded from the analysis. Ordinary one-way analysis of variance (ANOVA) followed by Turkey multiple comparison test was used to determine statistically significant differences between groups. If the Brown-Forsythe or the Bartlett's test indicated significantly different standard deviations, data were transformed to logarithms to accomplish variance homogeneity. $P < 0.05$ was considered statistically significant.

4. Results

4.1. Effect of monosaccharides on triglyceride accumulation, lipid localization as well as lipid droplet size and count in *C. elegans*

To investigate the effects of chronic exposure to monosaccharides in growth media on fat storage in *C. elegans* both, extraction-based biochemical and dye-based methods were employed.

Triglyceride concentration in nematodes maintained on growth media with added monosaccharides

To determine the effects of chronic exposure to 25 mM and 50 mM of fructose and glucose, respectively, on whole-body fat accumulation in *C. elegans* total TG were extracted from nematodes. Results of TG measurement in lipid extracts are summarized in Figure 12. TG concentration did not significantly differ between nematodes exposed to 25 mM of fructose or 25 mM of glucose and controls (F25: + 14 % and G25: + 31 % relative to controls, both $P > 0.05$). In contrast, exposure to both, 50 mM of fructose and 50 mM of glucose, resulted in significantly higher TG levels when compared to controls (F50: + 51 % and G50: + 57 % relative to controls, both $P < 0.01$).

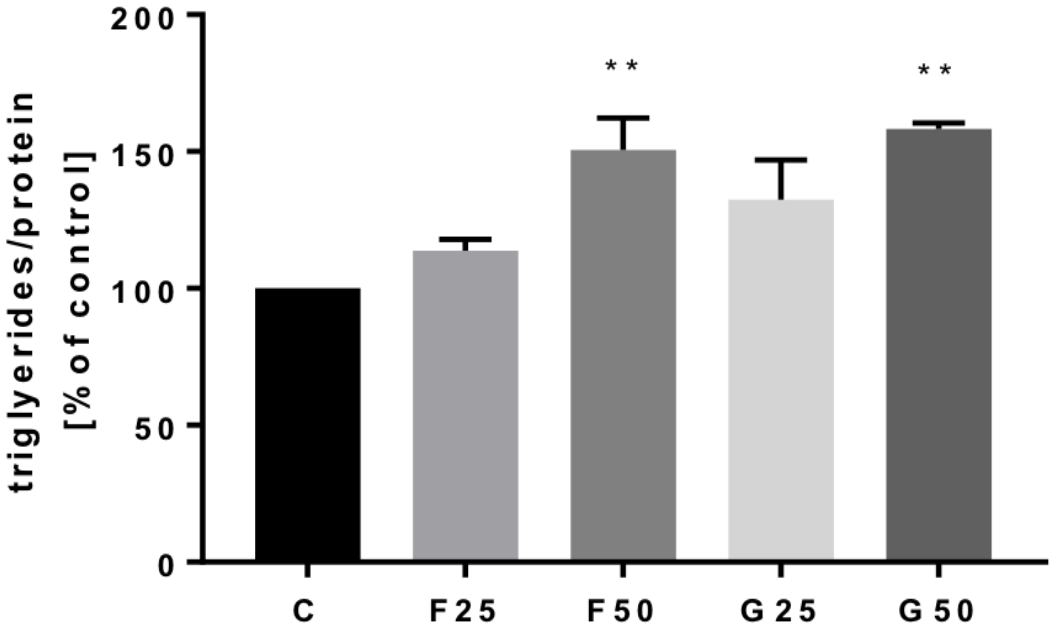

Figure 14: Effect of monosaccharides on triglyceride accumulation. *Nematodes were exposed to 25 mM and 50 mM of fructose and glucose, respectively, for a total of 4 days and TG concentration (mg triglycerides/μg protein) in lipid extracts from worm homogenates was determined as described in the methods section. Data are presented as means ± SEM. n = 4 independent experiments per treatment. TG and protein concentration were assayed in triplicates.* ** *P < 0.01 relative to control using one-way ANOVA.* ***Abbreviations:*** *C – control, F25 – 25 mM fructose, F50 – 50 mM fructose, G25 – 25 mM glucose, G50 – 50 mM glucose.*

Oil Red O staining in nematodes exposed to monosaccharides

C. elegans TG are stored in LD, which accumulate in the intestine, hypodermis, gonad, and eggs (75). To confirm the results of TG isolation and gain insights into LD number, size, and distribution in *C. elegans*, lipids were visualized by ORO staining. Results of the image-based quantification of staining are presented in Figure 13, representative photomicrographs of stained nematodes are displayed in Figure 14, and quantitative image analysis of LD size and count is summarized in Figure 15A – B. In line with the findings for TG isolation, exposure to 25 mM and 50 mM of fructose and glucose, respectively, resulted in a significantly higher percentage of ORO-stained areas within worms when compared to controls (F25: + 50 %, F50: + 49 %, G25: + 58 %, and G50: + 61 % relative to controls, all $P < 0.001$). Elevated lipid deposition correlated with a marked enlargement of LD in the intestine, but also in the hypodermis and the gonad of nematodes exposed to monosaccharides. Consistent with microscopic observation, quantitative image analysis showed that average LD size of worms treated with 25 mM of glucose was significantly higher than average LD size of controls (G25: + 97 % relative to controls, $P < 0.05$), while average LD size of worms treated with 25 mM of fructose did not significantly differ from controls (F25: + 48 % relative to controls, $P > 0.05$). In contrast, exposure to both, 50 mM of glucose and 50 mM of fructose, resulted in a significantly higher average LD size when compared to controls (G50: + 105 % and F50: + 86 % relative to controls, both $P < 0.05$). Furthermore, LD count was similar between all treatment groups (F25: – 10 %, F50: – 13 %, G25: – 15 %, and, G50: – 13 % relative to controls, all $P > 0.05$).

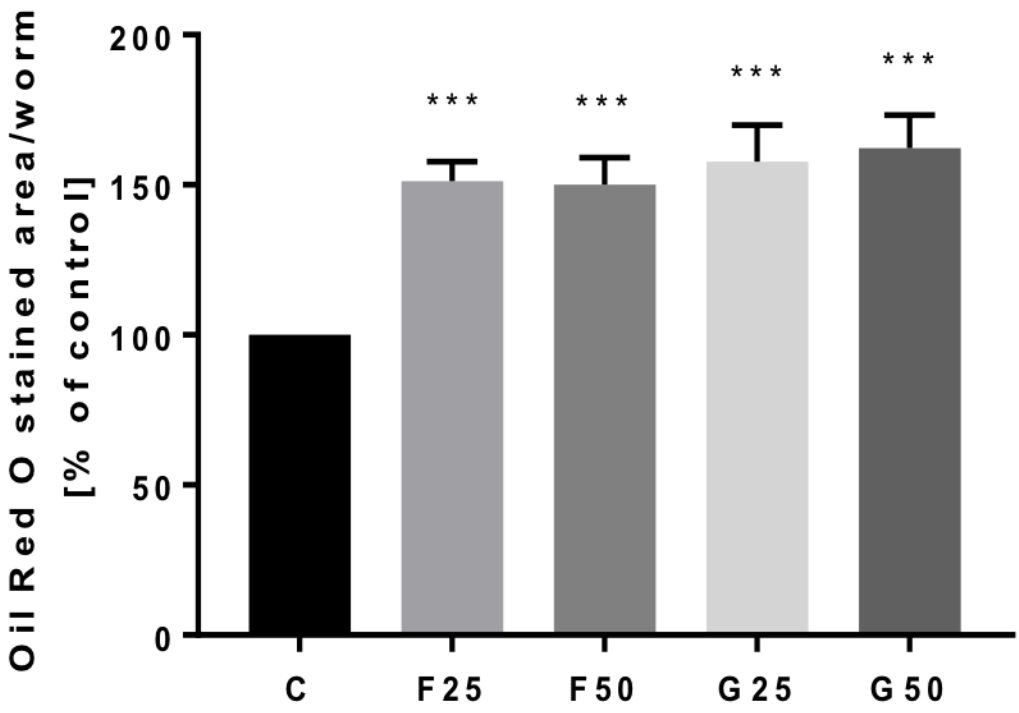

Figure 15: Effect of monosaccharides on Oil Red O staining. *Nematodes were exposed to 25 mM and 50 mM of fructose and glucose, respectively, for a total of 4 days. Lipid deposits were visualized by ORO staining and stained areas within worms were calculated as described in the methods section. Results are displayed as mean percentage of control ± SEM. n = 4 independent experiments with 10 – 15 animals per treatment.* *** *P < 0.001 compared to control using one-way ANOVA. Abbreverations: C – control, F25 – 25 mM fructose, F50 – 50 mM fructose, G25 – 25 mM glucose, G50 – 50 mM glucose.*

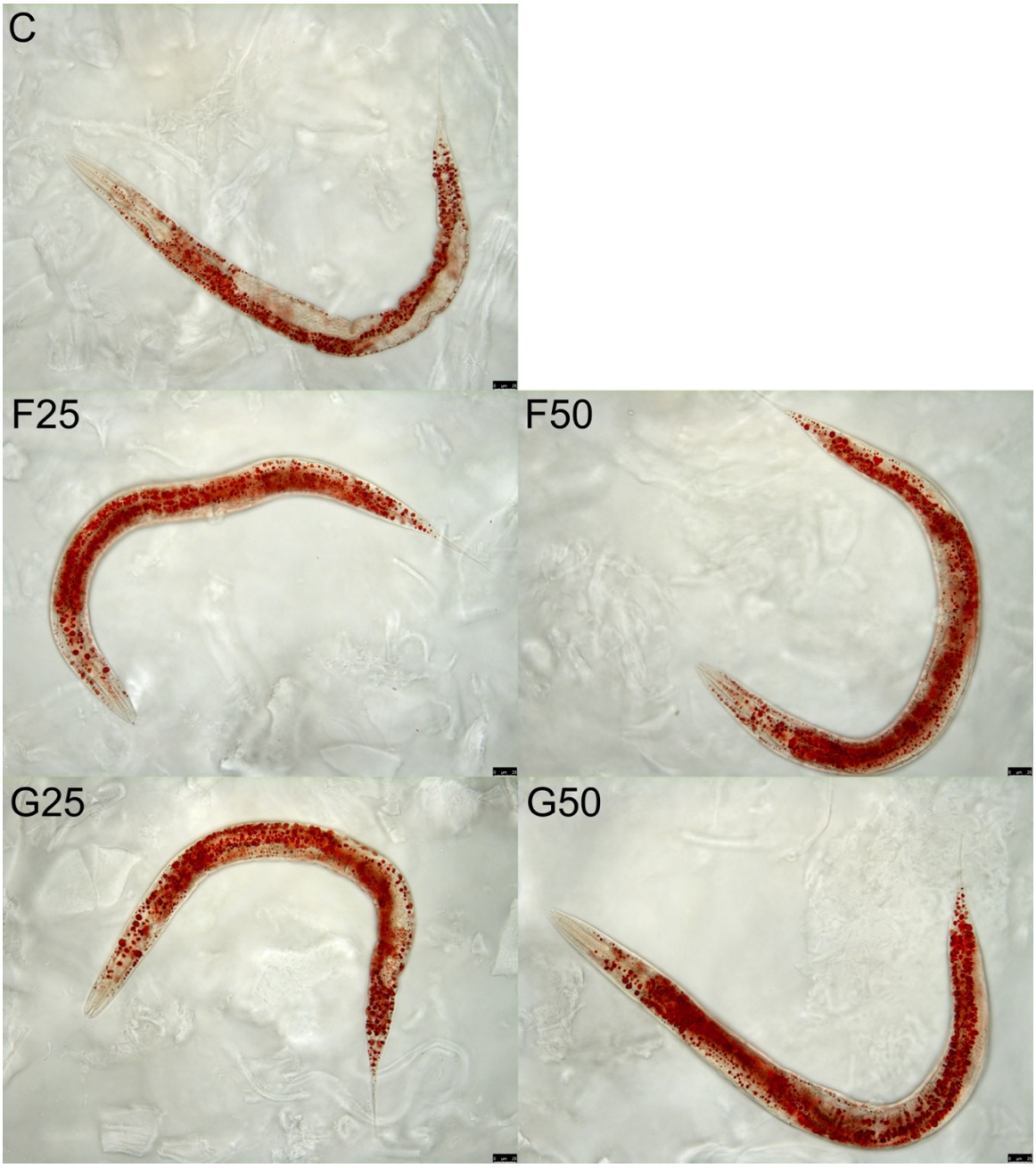

Figure 16: Effect of monosaccharides on lipid distribution. *Nematodes were exposed to 25 mM and 50 mM of fructose and glucose, respectively, for a total of 4 days and lipid deposits were visualized by ORO staining as described in the methods section. Scale bar = 25 μm. Abbreverations: C – control, F25 – 25 mM fructose, F50 – 50 mM fructose, G25 – 25 mM glucose, G50 – 50 mM glucose.*

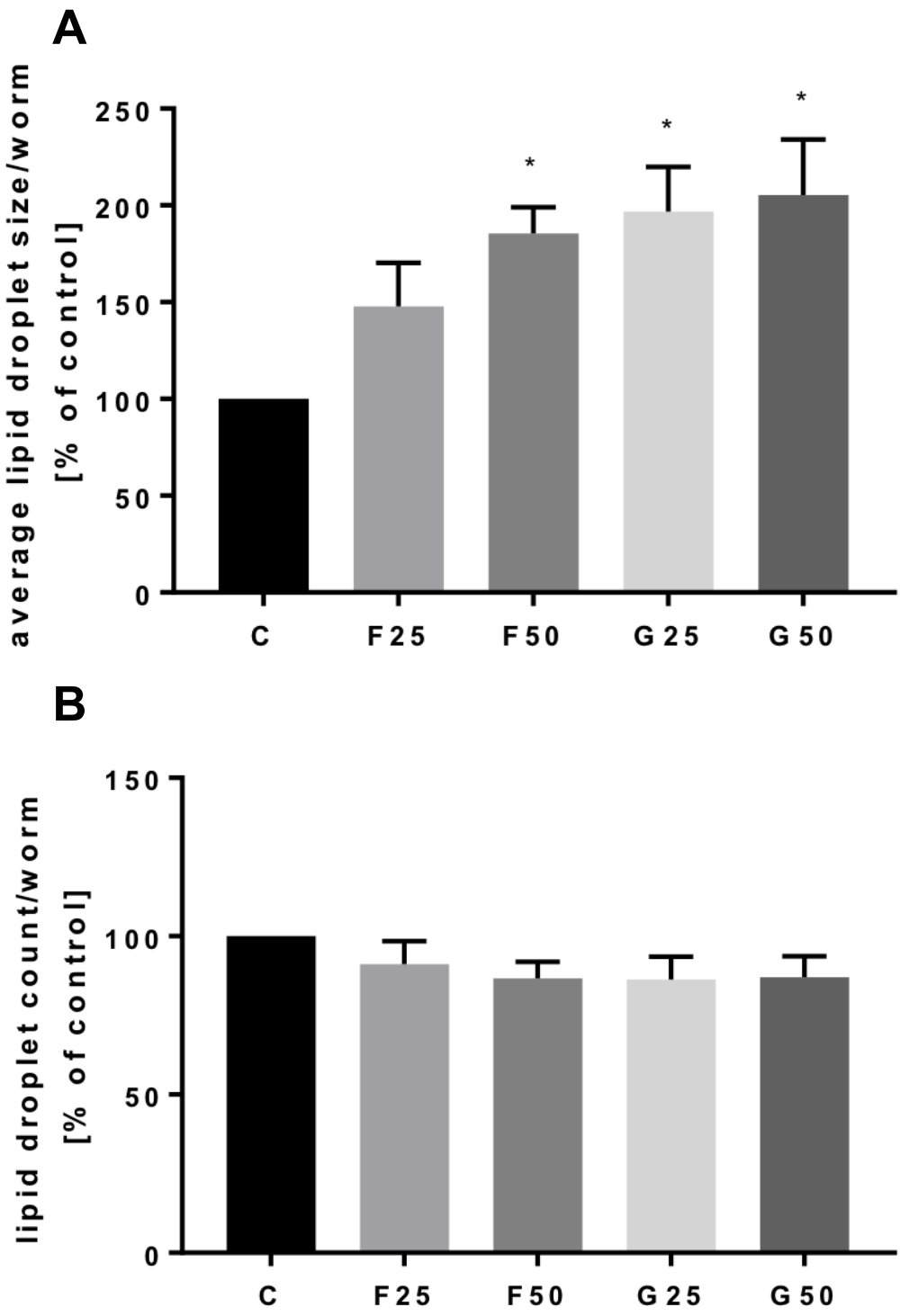

Figure 17: Effect of monosaccharides on lipid droplet size and count. *Nematodes were exposed to 25 mM and 50 mM of fructose and glucose, respectively, for a total of 4 days as described in the methods section. LD were visualized by ORO staining and (A) average LD size and (B) count were determined by quantitative image analysis. Results are presented as mean percentage of control ± SEM. n = 4 independent experiments, each with 10 – 15 animals per treatment.* * *P < 0.05 compared to control using one-way ANOVA. Abbreverations: C – control, F25 – 25 mM fructose, F50 – 50 mM fructose, G25 – 25 mM glucose, G50 – 50 mM glucose.*

4.2. Effect of monosaccharides on intestinal permeability and mRNA expression of *C. elegans* apical junction proteins

As studies in rodent models of NAFLD have repeatedly shown that chronic intake of a diet high in fructose but not glucose is associated with an increase in intestinal permeability (52,59) and a concomitant loss of TJ proteins in the small intestine (59,64), the influence of monosaccharides on intestinal barrier function and mRNA expression of proteins related to TJs in vertebrates was assessed in *C. elegans.*

Intestinal permeability of nematodes maintained on growth media with added monosaccharides

C. elegans intestinal barrier function was analyzed using a non-invasive dye-leakage assay. Figure 16 shows representative photomicrographs of nematodes after 3 h of incubation in liquid bacterial culture mixed with non-absorbable blue food dye. Dye was clearly visible in the intestinal lumen of *C. elegans.* However, neither worms exposed to 25 mM and 50 mM of fructose nor 25 mM and 50 mM of glucose exhibited any marked dye-leakage into the body cavity.

C. elegans apical junction protein expression in nematodes exposed to monosaccharides

To confirm the results of the intestinal barrier function assay, mRNA expression of ZO ortholog ZOO-1 as well as claudin homolog CLC-1 was assessed in *C. elegans*. RT-qPCR data are summarized in Figure 17. Neither exposure to 25 mM and 50 mM of fructose nor 25 mM and 50 mM of glucose altered mRNA expression of *zoo-1* (F25: – 49 % and F50: + 10 %, G25: + 4 % and G50: + 13 % relative to controls, all $P > 0.05$). Furthermore, mRNA expression of *clc-1* was similar between treatment groups (F25: + 136 %, F50: + 51 %, G25: + 56 %, and G50: + 277 % relative to controls, all $P > 0.05$).

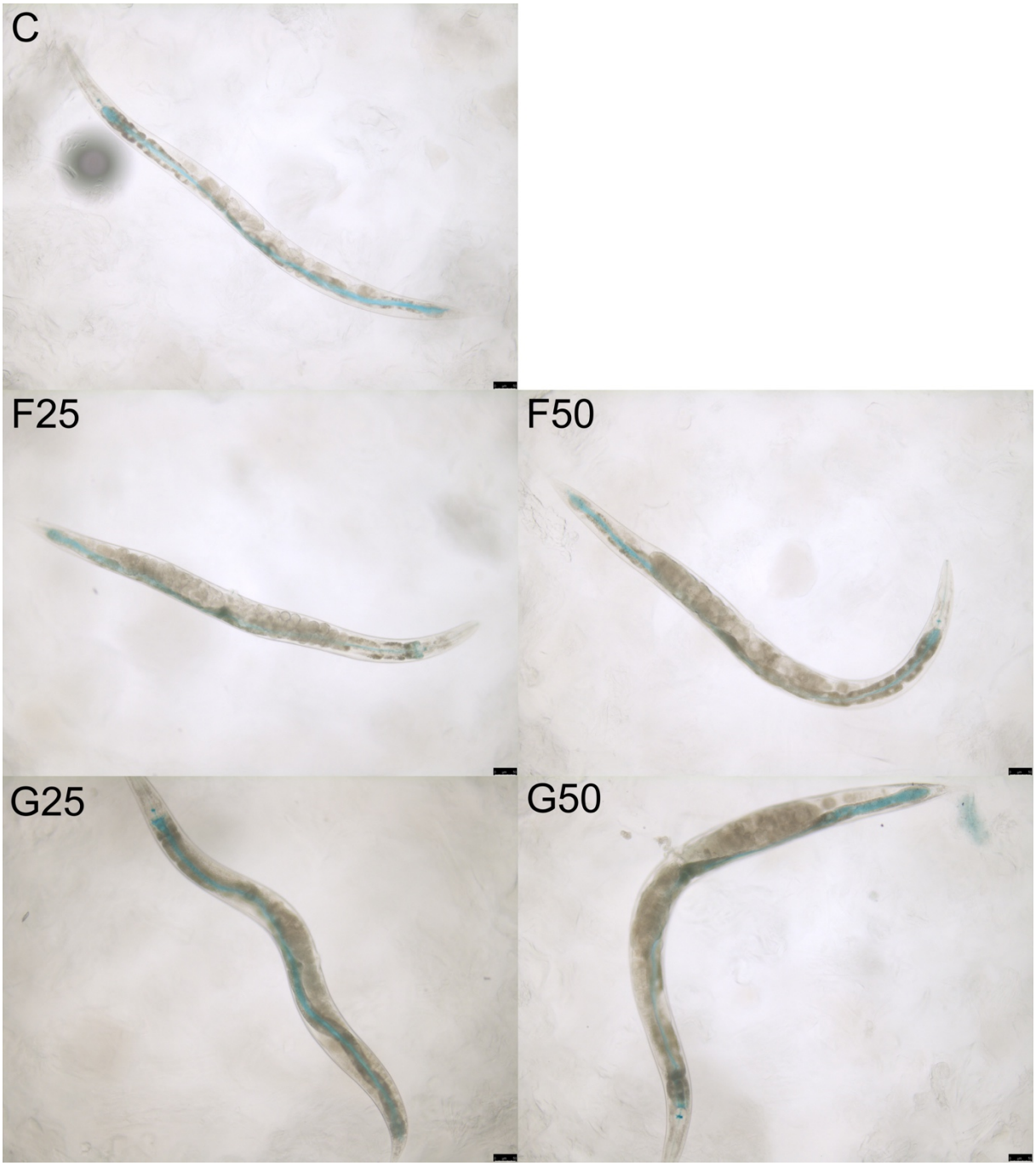

Figure 18: Effect of monosaccharides on intestinal dye-leakage. *Nematodes were exposed to 25 mM and 50 mM of fructose and glucose, respectively, for a total of 4 days. Subsequently, 10 animals per treatment were submerged in blue food dye for 3 h and analysed for intestinal dye-leakage into the body cavity. Scale bar = 50 μm. Abbreverations: C – control, F25 – 25 mM fructose, F50 – 50 mM fructose, G25 – 25 mM glucose, G50 – 50 mM glucose.*

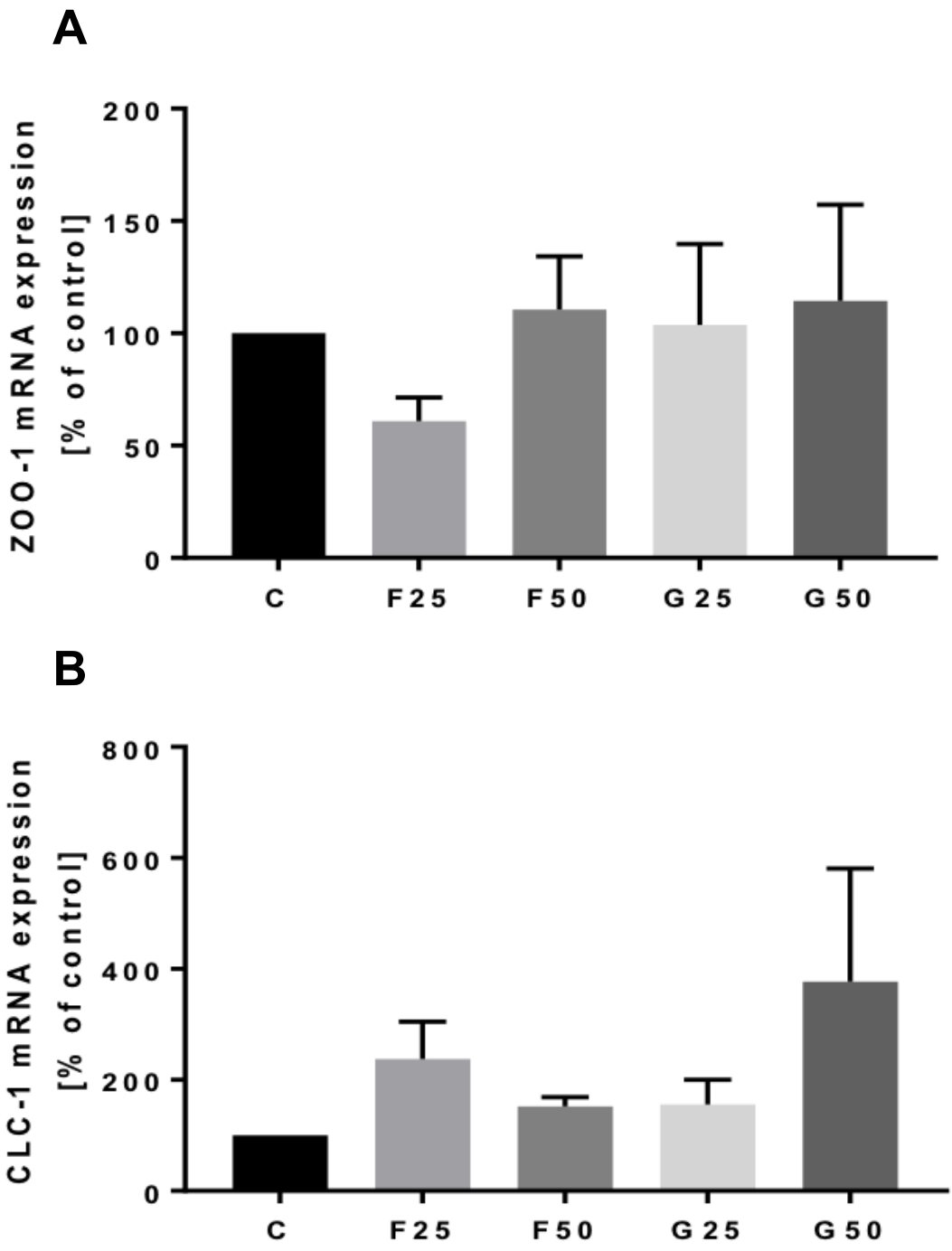

Figure 19: Effect of monosaccharides on mRNA expression of C. elegans apical junction proteins. *Worms were exposed to 25 mM and 50 mM of fructose and glucose, respectively, for a total of 4 days as described in the methods section. mRNA expression of (A) zoo-1 and (B) clc-1 was determined by RT-qPCR and normalized to mRNA expression of cdc-42. Results are presented as mean percentage of control ± SEM. n = 4 independent experiments per treatment. mRNA expression was assayed in duplicates. Abbreviations: C – control, F25 – 25 mM fructose, F50 – 50 mM fructose, G25 – 25 mM glucose, G50 – 50 mM glucose.*

5. Discussion

Lifestyle and especially dietary pattern have changed markedly over the past century, paralleled by an increase in the prevalence of obesity (98) and metabolic diseases (99), including NAFLD (100). As the etiology of many metabolic disease yet remains to be fully elucidated, therapeutic options are still limited (99). Therefore, a better understanding of the molecular mechanism underlying the onset and progression of metabolic disease is desirable to improve disease prevention and therapy.

Experimental evidence from studies in animal models (60) as well as meta-analyses basing calculations on RCTs in humans (3,4) indicates that excess sugar consumption may promote the development of obesity and metabolic disease. Despite the most commonly consumed sugars in Westernized countries constitute to near-equal proportions of fructose and glucose (5), research has recently focused on fructose, given its predominantly hepatic metabolism (15,16) and highly lipogenic potential (for an overview, see ref. (28,122)).

Indeed, studies in rodents (35,52,66) have shown that high-fructose diets compared with isocaloric diets rich in glucose increase lipid deposition in the liver. Fructose-induced hepatic steatosis was related to distinct changes in gut microbiota composition (59,64) as well as a loss of TJs in the upper parts of the small intestine (66,67,123), resulting in an elevated translocation of bacteria-derived pro-inflammatory molecules, notably endotoxin, into the portal vein (52,66) and an induction of TLR-dependent signaling pathways in the liver (54,67). Endotoxin-dependent activation of the TLR4 signaling cascade in hepatic Kupffer cells has been suggested to induce the synthesis and secretion of pro-inflammatory cytokines and ROS which, in turn, may interfere with hepatic lipid metabolism and insulin signaling, resulting in ectopic lipid deposition and insulin resistance (53). In line with these findings, concomitant treatment of fructose-fed mice with probiotics (57,58) or non-resorbable antibiotics (52,124) attenuated fructose-induced hepatic steatosis and inflammation, supporting a role for gut microbiota and intestinal barrier in fructose-induced metabolic alternations (125).

Many metabolic and molecular pathways are highly conserved between *C. elegans* and humans (73). In addition, *C. elegans* provides several inherent advantages as a

model organism, including its short lifespan, large brood sizes, ease of cultivation, and low maintenance expenses (for an overview, see ref. (70,71)). Therefore, the aim of the present study was to assess, if chronic exposure to fructose and glucose, respectively, in growth media also increases fat accumulation in *C. elegans* and if so, whether this is associated to a loss of proteins related to TJs in vertebrates.

5.1. Effect of monosaccharides on fat storage

Both, higher doses of fructose and glucose, respectively, induce a comparable increase in triglyceride accumulation in C. elegans

Studies in higher animal models indicate that an elevated fructose intake or bioavailability to the liver may promote DNL (32,33) and the subsequent development of fatty liver (52,123). While glucose has been extensively studied in *C. elegans* (126–130), research on the effects of fructose exposure on fat accumulation in *C. elegans* is rather scarce (131). Also, studies so far have been conducted under various experimental conditions (126). Differences in study protocols, including the types and concentrations of monosaccharides added to solid or liquid growth media as well as the methods employed for assessment of fat mass in *C. elegans*, make it difficult to compare the results obtained by different researchers in the field. In addition, studies have shown that WT *C. elegans* strains from different laboratories can feature a high degree of variability (132), possibly resulting in a differential response of nematodes to monosaccharides in growth media.

Results of TG isolation from worms indicate that TG accumulation in *C. elegans* is unaffected by lower concentrations of fructose or glucose in growth media, while higher concentrations of both monosaccharides significantly increase TG accumulation in *C. elegans*. Contrary to previous studies of Bergheim *et al.* (52), Haub *et al.* (66), as well as Roglans *et al.* (35) but consistent with recent rodent studies from others (32,33,103) the present data do not provide evidence for a differential effect of fructose and glucose regarding TG accumulation in *C. elegans.*

Considering that the majority of FA incorporated into *C. elegans* TG are directly obtained from bacterial diet and not DNL (80,81), it is possible that bacterial utilization of monosaccharides has abolished specific effects of fructose regarding TG accumulation in *C. elegans* (133). Indeed, Fraenkel *et al.* provided evidence for the existence of alternative routes of fructose utilization in *E. coli* (134).

Alternatively, differences between treatments may have been too small to detect with a colorimetric assay using an enzymatic method or variation between study replicates was too large for differences to reach statistical significance. Potential sources of variation between study replicates include bacterial cell concentration in 2X *E. coli* OP50 suspensions, number of plates and animals per plate as well as efficiency of lipid extraction and purification.

Image-based Oil Red O quantification correlates with biochemically measured triglyceride concentration in C. elegans

Extraction-based biochemical methods yield whole-organism, population-based measurements of fat mass but do not provide information regarding lipid localization in *C. elegans* (78). Consequently, processes, which lead to the redistribution of lipids to different tissues and subcellular compartments are obscured, when fat accumulation in *C. elegans* is only assessed using biochemical 'bulk' analyses (78,79).

To confirm the results of TG isolation from worm homogenates and gain insights into lipid distribution, lipids were visualized by ORO staining. ORO stains TG and other neutral lipids consistently and reproducibly (114). In line with TG isolation, image-based quantification of ORO staining showed a comparable increase in lipid deposition in nematodes maintained on growth media with added fructose or glucose yet no dose-response relationship between monosaccharide concentration in growth media and fat accumulation in *C. elegans* was found.

Although several studies demonstrated that ORO quantification correlates with biochemically measured TG concentration in *C. elegans* (75,135), the precision of ORO staining for the quantitative assessment of fat mass in *C. elegans* is

controversially discussed (79). Compared with biochemical assays, which measure major classes of lipids or individual FA directly after lipid extraction from worm homogenates, fixative-based staining methods provide only indirect measurements of fat mass and are prone to large intrasample variability and low sensitivity associated with non-uniform permeabilization of the cuticle (78).

Although TG isolation and ORO staining did not yield absolutely congruent results, the correlation between the results obtained by both methods indicates that image-based ORO quantification can indeed serve as a proxy for fat mass in *C. elegans* (75). However, considering the fact that fertility and age can modulate fat mass and distribution in *C. elegans* (114), nematodes may need to be selected according to developmental stage in order to increase the accuracy of results.

Studies have repeatedly shown that even lower doses of glucose decrease brood size of *C. elegans* and accelerate aging (126,128,130). In contrast, lower concentrations of fructose have recently been associated with an increase in lifespan of *C. elegans,* inversely related to intestinal lipid deposition (131). Consistent with the literature, brood size of nematodes treated with glucose appeared to be reduced, while fructose exposure seemed to increase progeny production, which is a new finding. Fertility and age are known modulators of fat mass and lipid distribution in *C. elegans* (114). Thus, it is possible that the differential effect of fructose and glucose on fertility and age has confounded the effect of both monosaccharides on fat accumulation in *C. elegans*. However, as quantitative analysis of lifespan and brood size was beyond of the scope of this study, further studies are necessary to confirm these observations.

Elevated fat accumulation in C. elegans is associated with an enlargement of lipid droplets in the intestine of C. elegans

Similar like in mammalians, *C. elegans* lipids are distributed among diverse tissues and subcellular compartments, where lipids likely exert very different functions (78). While, the major proportion of lipids is located in the intestine and the proximal gonad of WT worms, a substantial fraction of lipids is also contained in the embryos of gravid hermaphrodites (79). To date it is unknown which lipid stores or proportion of total

lipids from *C. elegans* are transient (e.g. intended for reproduction or tissue maintenance) versus being stored (78). However, based on its function in lipid and lipoprotein metabolism, it has been hypothesized that the intestine of *C. elegans* is a liver-like tissue, while the hypodermis may function as a long term energy storage site analogous to the human adipose tissue (78).

ORO staining is regarded as a reliable method for the assessment of lipid localization in *C. elegans* (114). Microscopic observation of stained nematodes showed a marked enlargement of LD in the intestine of nematodes maintained on growth media with added fructose or glucose, possibly reflecting elevated hepatic lipid deposition previously observed in rodents (32,33,103). In addition, enlarged LD were observed in the hypodermis as well as the proximal gonad of nematodes treated with monosaccharides, suggesting that lipids from the intestine were exported to extraintestinal tissues (77).

A major study limitation is that tissue-specific changes in fat mass were not quantified, raising the possibility that tissue-specific treatment effects were underestimated. Considering the fact that several studies reported a differential effect of fructose and glucose on lipid distribution across tissues such as the liver and the adipose tissue (36,52), future studies should focus on lipid localization rather than fat mass, using a tissue-specific approach for the analysis of lipids (79).

However, quantitative image-analysis confirmed an increase in average LD size in nematodes treated with fructose or glucose, while LD count was unaffected by both monosaccharides. LD hypertrophy in intestinal and hypodermal cells has been related to elevated DNL in *C. elegans* (84) and is considered a hallmark of obesity and hepatic steatosis in mammalians (136,137). Notably, LD enlargement appeared to be more pronounced in nematodes exposed to glucose in growth media. However, differences between treatments did not reach statistical significance.

5.2. Effect of monosaccharides on markers of intestinal barrier function

Both, diets high in fructose and glucose, respectively, are not associated with an increase in intestinal permeability in C. elegans

Studies in rodent models of NAFLD have repeatedly shown that fructose-induced metabolic alternations are associated with a disruption of intestinal integrity, resulting in an increase in intestinal permeability and an elevated translocation of gut-derived pro-inflammatory molecules such as endotoxin into portal plasma (59,64,66,123). Despite the fact that the intestine of *C. elegans* consists of only 20 cells, key anatomical features of the intestinal epithelium are conserved between *C. elegans* and humans (for an overview, see ref. (86)). In addition, the transparent body wall of *C. elegans* aids the microscopic observation of the intestine *in vivo* (138).

To investigate whether elevated lipid deposition in nematodes treated with monosaccharides is associated with a decrease in intestinal barrier function, nematodes were cultured on NGM plates with 25 and 50 mM of fructose and glucose, respectively, as described previously and intestinal permeability was assessed with a non-invasive dye-leakage assay (115), termed the 'Smurf' assay (116,139). The Smurf assay allows direct *in vivo* assessment of intestinal barrier function by the co-ingestion of blue dye, which is not absorbed by the digestive system of *C. elegans*. Animals, which exhibit whole-body coloration, are classified as 'Smurfs' (140).

Contrary to what was expected based on studies in higher animal model, microscopic observation of nematodes after 1, 3 and 6 h of feeding by incubation in liquid bacterial culture mixed with non-resorbable blue food dye did not provide evidence for a significant increase in dye-leakage from the intestinal lumen into the body cavity of nematodes treated with 25 and 50 mM of fructose and glucose, respectively, suggesting that intestinal permeability is unaffected by the two monosaccharides investigated in this study.

Despite described as simple, the Smurf assay imposes several challenges when implementing. Most importantly, the Smurf phenotype is contiguous, which bears the risk that animals are misclassified as Smurfs, when phenotypic variation is minimal (140). Therefore, it is possible that the treatment effects were too small to be detected with the Smurf assay.

In addition, despite *C. elegans* lifecycle is rapid (approximately 3 days at 25 °C, for an overview, see ref. (71)), it cannot be ruled out that the incubation time was too short to induce marked alternations in *C. elegans* intestinal barrier function. Indeed, Gelino *et al.* (115) reported a specific increase in intestinal permeability around mid-adulthood, raising the possibility that the window of exposure to monosaccharides (around early-adulthood) was inappropriate to detect marked alternations in *C. elegans* intestinal barrier function.

Diets high in fructose and glucose, respectively, are both not associated with a reduced mRNA expression of C. elegans apical junction proteins

Intestinal permeability in vertebrates is regulated by the expression of TJ proteins such as claudins and ZO-1 (141). *C. elegans* epithelia do not bear typical TJs but instead harbor a single large apical junction, termed the *C. elegans* apical junction (CeAJ), which has features of both, AJs and TJs (91). To verify the results obtained by the Smurf assay, RNA was isolated from worm homogenates and mRNA expression of *C. elegans* claudin homologue *clc-1* as well as ZO orthologue *zoo-1* was determined by RT-qPCR. Analysis of RT-qPCR data did not provide evidence for a reduced mRNA expression of CeAJ proteins in nematodes treated with monosaccharides, confirming the results obtained by the Smurf assay.

Notably, CeAJ protein expression was only assessed at the level of transcription. Therefore, alternations in CeAJ protein translation or posttranslational modification cannot be excluded. Indeed, Volynets *et al.* (59) documented no significant alternation in the mRNA expression of TJ proteins in a rodent model of fructose-induced NAFLD, while, protein expression was found to be significantly reduced.

In addition, studies reported a selective loss of TJ proteins in the upper part of the small intestine of mice (59,123) and human patients with NAFLD (142), but not in more distal parts, indicating that orally ingested fructose may affect TJ protein expression only in specific intestinal compartments. Claudin-like protein CLC-1 is primarily expressed in the pharyngeal epithelium of the digestive tube of *C. elegans* (94), while ZOO-1 is actively expressed in intestinal but also in hypodermal epithelial cells (91), raising the possibility that tissue-specific changes in the mRNA expression of CeAJ proteins were obfuscated because gene expression was only determined on organismal level.

To the authors knowledge, this is the first study to investigate and compare the effects of fructose and glucose exposure, respectively, on intestinal barrier function in the *C. elegans* model, thus further studies are certainly necessary to verify the present results. Reasons for the discrepancies between the current findings and those obtained in rodent studies are unknown but might be related to the limited applicability of the *C. elegans* model for the study of fructose-induced intestinal barrier dysfunction and associated metabolic alternations.

Fructose-induced NAFLD has been related to distinct changes in gut microbiota composition (64,124,125). Bacteria in the gut lumen can modulate *C. elegans* physiology independent of their role as a food source analogous to the gut microbiota in vertebrates (89,90) (for an overview, see ref. (88)). However, whether something akin to microbiota dysbiosis exists in nematodes maintained in monoxenic culture with *E. coli* OP50 is still an open research question (88).

Furthermore, *C. elegans* epithelia do not bear typical TJs but instead harbor a single large apical junction, which has features of both, AJs and TJs (91). A distinctive feature of the CeAJ is that ZOO-1, the sole *C. elegans* orthologue of the ZO family, localizes to the cadherin-catenin complex (CCC) and *zoo-1* loss-of-function mutations do not result in a disruption of the epithelial barrier. These findings indicate that ZOO-1 is not required for the maintenance of paracellular permeability in *C. elegans* (97).

Moreover, *C. elegans* lacks an innate immune system comparable to those of vertebrates (143). Although many signaling pathways, including the TGF-β as well as

the p38 MAPK pathway, are highly conserved between *C. elegans* and humans, others, such as the TLR and JAK/STAT signaling pathway, are only partially conserved or thought to be completely absent (144). Most importantly, the genome of *C. elegans* does not encode homologues for the transcription factor NFκB as well as the TLR adaptor protein MyD88, and known vertebral cytokines (138), which are believed to mediate the effect of endotoxin in the liver of fructose-fed mice (53,54). However, recent work in rodent models suggests that fructose has a specific detrimental effect on metabolic outcome parameters even in the absence of intestinal barrier dysfunction and metabolic endotoxinemia (145).

Besides time and height, form of exposure to monosaccharides may have influenced the effects of fructose and glucose, respectively, on fat accumulation and intestinal barrier function in *C. elegans*. Indeed, studies have shown that solid versus liquid formulations of fructose differentially affect intestinal barrier function and hepatic TG accumulation in mice (146). Thus, considering the inherent limitations of the present study, including limited exposure time, small range of monosaccharide concentrations tested, exposure to monosaccharides in solid versus liquid growth media as well as ample supply of bacteria, the present findings may be viewed as preliminary.

6. Conclusion

Taken together, the results of the present study suggest that chronic exposure to higher concentrations of fructose or glucose in growth media induce a comparable increase in TG accumulation in *C. elegans*, associated with a marked enlargement of LD in major *C. elegans* lipid storage organs, notably along the intestine. The present data also indicate that elevated lipid deposition in nematodes maintained on growth media with added monosaccharides is not associated with an increase in intestinal permeability or a reduced mRNA expression of proteins related to TJs in vertebrates, suggesting that other mechanism may be involved in the observed increase in *C. elegans* lipids. Since evidence form studies in mice (52) and humans (36) suggests that fructose and glucose differentially affect lipid distribution, further studies on the influence of dietary monosaccharides on fat accumulation in *C. elegans* should focus on lipid localization rather than fat mass, using a tissue-specific approach for the assessment of *C. elegans* fat stores. These studies should include measures of brood size and lifespan to clarify whether dietary monosaccharides differentially affect *C. elegans* fertility and age and if this impinges on fat mass and distribution as well as intestinal barrier function.

7. Summary

Chronic, high-fructose intake has been implicated in the onset and progression of metabolic disease, especially non-alcoholic fatty liver disease (NAFLD). Evidence from studies in the rodent models further suggests that fructose-induced metabolic alternations are associated with a loss of tight junction (TJ) proteins in the upper parts of the small intestine, resulting in an elevated translocation of gut-derived pro-inflammatory molecules, notably endotoxin, into the portal vein and an induction of the Toll-like receptor 4 (TLR-4) signaling cascade in the liver. Endotoxin-dependent activation of hepatic Kupffer cells is assumed to increase the synthesis and secretion of pro-inflammatory cytokines such as tumor necrosis factor-α (TNF-α), which, in turn, may dysregulate hepatic glucose and lipid metabolism, resulting in ectopic lipid deposition and insulin resistance.

Starting from this background the aim of the present master thesis was to assess the effects of a fructose or glucose rich diet on fat accumulation and TJ integrity in the *Caenorhabditis elegans* (*C. elegans*) model. Therefore, wildtype nematodes were exposed to 25 mM and 50 mM of fructose and glucose, respectively, in growth media for a total of 4 days. *C. elegans* fat mass was quantified by lipid extraction from worm homogenates and colorimetric assessment of triglyceride (TG) concentration in lipid extracts. In addition, *C. elegans* lipid deposits were visualized by Oil Red O (ORO) staining to gain insights into lipid localization as well as lipid droplet (LD) size and count. Higher doses of fructose and glucose, respectively, induced a comparable increase in TG accumulation in *C. elegans*. Elevated TG stores correlated with a higher percentage of ORO stained areas within worms. Lipid deposits were observed in the intestine but also in the hypodermis and the proximal gonad of nematodes treated with monosaccharides. Exposure to monosaccharides further resulted in a significantly higher average LD size when compared with controls, while LD count was similar between treatment groups.

To clarify whether elevated lipid deposition in nematodes exposed to monosaccharides was associated with a disruption of TJ integrity, *C. elegans* intestinal barrier function was assessed with a non-invasive dye-leakage assay. In addition, mRNA expression

of *zonula occludens* (ZO) orthologue *zoo-1* as well as claudin homologue *clc-1* was quantified by real-time quantitative PCR (RT-qPCR). Neither 25 mM and 50 mM of fructose nor 25 mM and 50 mM of glucose resulted in any marked dye-leakage from the intestinal lumen into the body cavity of *C. elegans*. In consistence, mRNA expression of *zoo-1* as well as *clc-1* was unaffected by dietary monosaccharides.

Taken together the results of the present master thesis suggest that, both fructose and glucose at higher doses can increase fat accumulation in *C. elegans* without a concomitant loss of proteins related to TJs in vertebrates. However, further studies are necessary to verify the present findings and to clarify whether fructose and glucose induce tissue-specific changes in *C. elegans* fat mass and distribution as well as intestinal barrier function or impact on other physiological variables, which may confound the effects of monosaccharides on fat storage and intestinal barrier.

Annex

Preparation of media and buffer

LB agar

The following reagents are blended in a screw-cap bottle, diluted with 1000 ml ddH_2O and sterilized by autoclaving:

LB agar (g)	10.0
LB broth (g)	20.0

Once LB agar has cooled down to 50 °C in the water bath, it is aseptically poured into sterile petri dishes (25 ml/plate). LB plates that have solidified and dried are sealed with petri film and stored at 4 °C.

DYT media

The following ingredients are blended in a screw-cap bottle and diluted with 1000 ml ddH_2O:

Tryptone/Peptone (g)	16.0
Yeast extract (g)	10.0
NaCl (g)	5.0

DYT media is sterilized by autoclaving and stored at 4 °C.

2.5 M sugar stock solutions

Fructose or glucose (g)	4.504

5.0 M sugar stock solutions

Fructose or glucose (g)	9.008

Monosaccharides are dissolved in 10 ml ddH_2O and filtered through a 20-µm filter.

NGM agar

The reagents listed below are mixed in a screw-cap bottle, diluted with 1000 ml ddH_2O and sterilized by autoclaving:

NaCl (g)	3.0
Tryptone/Peptone (g)	2.5
Agar-Agar (g)	17.0

After cooling down to 50 °C in the water bath, NGM agar is blended with the following ingredients:

1M $CaCl_2$ (ml)	0.5
5 mg/mL Cholesterol in ethanol (ml)	1.0
1M $MgSO_4$ (ml)	1.0
1M Potassium phosphate buffer pH 6 (ml)	25.0
Nystatin (ml)	5.0

NGM agar for experimental purpose is supplemented with 100-times concentrated sugar stock solutions or sterile water. To reach a final concentration of 25 mM and 50 mM, respectively, the volume added by the NGM ingredients and the test substances is removed prior to the addition of the sugar stock solutions:

Volume correction (ml)	42.5
Sugar stock solution or sterile water (ml)	10.0

NGM agar is aseptically poured into sterile petri dishes (20 ml/plate).
Once NGM plates have solidified and dried, they are sealed with petri film and stored at 4 °C.

S buffer

NaCl (g)	5.85
0.05 M KH_2PO_4 (ml)	871
0.05 M $K_2HPO_4 \cdot 3H_2O$ (ml)	129

NaCl is dissolved in 0.05 M KH_2PO_4 and 0.05 M $K_2HPO_4 \cdot 3H_2O$.

S buffer is sterilized by autoclaving and stored at 4 °C.

1M Potassium phosphate buffer (pH 6)

The following ingredients are dissolved in 1000 ml ddH_2O:

KH_2PO_4 (g)	108.53
$K_2HPO_4 \cdot 3H_2O$ (g)	46.22

Potassium phosphate buffer is sterilized by autoclaving and stored at 4 °C.

M9 buffer

The following ingredients are dissolved in 1000 ml ddH2O:

KH_2PO_4 (g)	3.0
Na_2HPO_4 (g)	6.0
NaCl (g)	5.0
1 M $MgSO_4$ (ml)	1.0

M9 buffer is sterilized by autoclaving and stored at 4 °C.

10X PBS (pH 7.4)

The following ingredients are dissolved in 1000 ml ddH_2O:

NaCl (g)	80.0
KCl (g)	2.0
Na_2HPO_4 (g)	7.62
KH_2PO_4 (g)	0.77

For the preparation of 2X PBS, 1 part of 10X PBS is diluted with 4 parts of ddH_2O.

5X TBE buffer

The following ingredients are diluted to a final volume of 1000 ml with ddH_2O:

TRIS (g)	54.0
Boric acid (g)	27.5
0.5 M EDTA (ml)	20.0

For the preparation of 1X TBE, 1 part of 5X TBE is diluted with 4 parts of ddH_2O.

Nystatin

CH_3COONH_4 (g)	57.81

Ammonium acetate is dissolved in 100 ml ddH_2O.

Ethanol, 96 % (ml)	100.0
Nystatin (g)	2.0

Nystatin is dissolved with the rotational addition of ammonium acetate in ddH_2O and 96 % ethanol to a final volume of 200 ml. The solution is heated for 1 h at 55 °C and subsequently filtered through a 20-µm filter.

Oil Red O stock solution

Oil Red O (mg)	500
Isopropanol (ml)	100

Oil Red O is suspended in isopropanol and equilibrated for 4 d while rocking at 100 rcf.

5 % (w/v) blue dye solution

Erioglaucine disodium salt (mg)	50.0

Erioglaucine disodium salt is dissolved in 1 ml sterile water.

For the preparation of 1 % (w/v) blue dye in liquid bacterial culture, 2X *E. coli* OP50 suspension is centrifuged for 30 min at maximum speed and 4 °C. Subsequently, the supernatant is removed, and bacteria are resuspended in 0.5 times the volume of S media. 4 parts of the suspension are then mixed with 1 part of 5 % (w/v) blue dye solution to reach a final concentration of 1% (w/v) blue dye in liquid culture.

5 % agarose pads

Agarose (mg)	500

Agarose is suspended in 10 ml ddH_2O and melted in a 65 °C water bath. 1 – 2 drops are placed on a clean glass slide framed by two taped glass slides. The tape will serve as a spacer flattening the drop to a 0.4 mm thick pad when a second clean glass slide is placed on top. Once the agarose pad has solidified, the taped glass slides are removed, and the top glass slide can be detached from the agar pad. Alternatively, agarose pads can be wrapped in plastic foil and used within 3 h.

Supplementary Tables

Supplementary Table 1: Number of plates and animals per plate.

	hermaphrodites	**L4 larvae**	**eggs**	**YA**	**adults**
plates	3	5 – 7	10 – 14	7 – 13	25 – 40
animals/plate	19 – 20	9 – 10	0	300 – 400	100 – 150

Supplementary Table 2: Dilution of triglycerides in 5 % BSA.

Trail	**5% BSA (µl)**	**Dilution**	**Factor**
1	100	–	2
2, 3, 4	200	1:2	1

Supplementary Table 3: Dilution of proteins in 2X PBS.

Trail	**2X PBS (µl)**	**Dilution**	**Factor**
1	100	1:5	5
2, 3, 4	250	1:2	2

Supplementary Table 4: Dilution of proteins in ddH_2O.

Trail	**Sample (µl)**	**Dilution**	**Factor**
1	15	1:3	3
2, 3, 4	25	1:10	10

Zusammenfassung

Eine fruktosereiche Diät wird als Risikofaktor für die Entstehung und Progression metabolischer Erkrankungen wie der nicht-alkoholbedingten Fettlebererkrankung (*non-alcoholic fatty liver disease,* NAFLD) diskutiert. Studien im Mausmodell deuten darauf hin, dass Fruktose-assoziierte Stoffwechselveränderungen mit einem Verlust von *tight junction* (TJ) Proteinen im oberen Dünndarm einhergehen. Der damit verbundene Anstieg der intestinalen Permeabilität wird als ursächlich für eine erhöhte Translokation bakterieller Endotoxine in die Pfortader und eine Induktion TLR-4-abhängiger Signalwege in der Leber vermutet. Dies könnte zur Aktivierung hepatischer Kupfferzellen und einer verstärkten Expression entzündlicher Zytokine wie dem Tumornekrosefaktor-α (*tumor necrosis factor*-α, TNF-α) führen, von denen angenommen wird, dass sie die Fettinfiltration in die Leber begünstigen und ihre Insulinsensitivität herabsetzen können.

Ausgehend von diesem Hintergrund war das Ziel der vorliegenden Arbeit den Einfluss einer fruktose- bzw. glukosereichen Diät auf die Fetteinlagerung und intestinale Barrierefunktion im *C. elegans* Modell zu untersuchen. Dazu wurden die Nematoden während einer viertägigen Interventionsperiode auf Agar-Platten mit 25 bzw. 50 mM Fruktose oder Glukose kultiviert. Die Bestimmung des Fettgehalts erfolgte mittels Extraktion der Lipide und kolorimetrischer Bestimmung der Triglyzeridkonzentration in den Lipidextrakten. Zusätzlich wurden die Fettdepots der Nematoden durch Abfärbung mit Oil Red O (ORO) visualisiert, um Informationen über die Fettverteilung, sowie Fetttröpfchengröße und -anzahl zu erhalten.

Sowohl Fruktose als auch Glukose führten in hohen Konzentrationen zu einem signifikanten Anstieg der Triglyzeridkonzentration in *C. elegans*. Die Ergebnisse der Triglyzeridbestimmung korrelierten mit jenen der ORO Färbung. Fettablagerungen fandens sich vor allem im Darm der Nematoden, jedoch auch in der Hypodermis und der Gonade. Darüber hinaus waren die Fetttröpfchen der Fruktose- bzw. Glukose-gefütterten Nematoden im Mittel signifikant größer als jene der Kontrollen, während die mittlere Anzahl der Fetttröpfchen nicht signifikant zwischen den Gruppen differierte.

Um abzuklären, ob die mit Fruktose- bzw. Glukoseaufnahme verbundene Zunahme der Fettakkumulation mit einer Störung der intestinalen Barrierefunktion einhergeht, wurde ein nicht-invasiver Permeabilitätstest durchgeführt und durch Messung der mRNA Expression des *C. elegans Zonula occludens* Orthologs ZOO-1 sowie des Claudin Homologes CLC-1 mittels quantitativer *real time* PCR validiert. Es zeigte sich keine signifikante Zunahme der intestinalen Permeabilität. In Übereinstimmung differierte die mRNA Expression von ZOO-1 und CLC-1 nicht signifikant zwischen den Gruppen.

Zusammenfassend deuten die Ergebnisse der vorliegenden Arbeit darauf hin, dass sowohl Fruktose als auch Glukose in hohen Konzentrationen die Fettakkumulation in *C. elegans* erhöhen können, wobei dies nicht mit einer Störung der intestinalen Barrierefunktion einhergeht. Es sind jedoch weitere Studien im *C. elegans* Modell erforderlich um die vorliegenden Ergebnisse zu validieren sowie abzuklären, ob es gewebespezifische Unterschiede in Fettablagerung und Barrierefunktion zwischen Fruktose- und Glukose-gefütterten Nematoden gibt bzw. andere Faktoren die Wirkung von Fruktose und Glukose auf Fettablagerung sowie Barrierefunktion im *C. elegans* Model beeinflussen könnten.

References

1. Rust P, Hasenegger V, König J. Österreichischer Ernährungsbericht 2017. 2017;169.
2. WHO. WHO | Sugars intake for adults and children [Internet]. WHO. 2015 [cited 2018 Aug 27]. Available from: http://www.who.int/nutrition/publications/guidelines/sugars_intake/en/
3. Te Morenga L, Mallard S, Mann J. Dietary sugars and body weight: systematic review and meta-analyses of randomised controlled trials and cohort studies. BMJ. 2012;346:e7492.
4. Te Morenga LA, Howatson AJ, Jones RM, Mann J. Dietary sugars and cardiometabolic risk: systematic review and meta-analyses of randomized controlled trials of the effects on blood pressure and lipids. Am J Clin Nutr. 2014;100:65–79.
5. White JS. Straight talk about high-fructose corn syrup: what it is and what it ain't. Am J Clin Nutr. 2008;88(suppl):1716S–1721S.
6. Smith Jr. LH, Ettinger RH, Seligson D. A comparison of the metabolism of fructose and glucose in hepatic diseases and diabetes mellitus. J Clin Invest. 1952;31:273–82.
7. Gorboulev V, Schürmann A, Vallon V, Kipp H, Jaschke A, Klessen D, Friedrich A, Scherneck S, Rieg T, Cunard R, et al. Na(+)-D-glucose cotransporter SGLT1 is pivotal for intestinal glucose absorption and glucose-dependent incretin secretion. Diabetes. 2012;61:187–96.
8. Burant CF, Takeda J, Brot-Laroche E, Bell GI, Davidson NO. Fructose Transporter in Human Spermatozoa and Small Intestine Is GLUT5. J Biol Chem. 1992;267:14523–6.
9. Gouyon F, Caillaud L, Carriere V, Klein C, Dalet V, Citadelle D, Kellett GL, Thorens B, Leturque A, Brot-Laroche E. Simple-sugar meals target GLUT2 at enterocyte apical membranes to improve sugar absorption: a study in GLUT2-null mice. J Physiol. 2003;552.3:823–32.
10. Jang C, Hui S, Lu W, Cowan AJ, Morscher RJ, Lee G, Liu W, Tesz GJ, Birnbaum MJ, Rabinowitz JD. The Small Intestine Converts Dietary Fructose into Glucose and Organic Acids. Cell Metab. 2018;27:351-361.e3.
11. Ockerman PA, Lundborg H. Conversion of fructose to glucose by human jejunum absence of galactose-to-glucose conversion. Biochim Biophys Acta. 1965;105:34–42.
12. DeFronzo RA, Ferrannini E. Regulation of hepatic glucose metabolism in humans. Diabetes Metab Rev. 1987;3:415–59.
13. Ferrannini E, Bjorkman O, Reichard GA, Pilo A, Olsson M, Wahren J, DeFronzo RA. The Disposal of an Oral Glucose Load in Healthy Subjects: A Quantitative Study. Diabetes. 1985;34.
14. Katz LD, Glickman MG, Rapoport S, Ferrannini E, DeFronzo RA. Splanchnic and Peripheral Disposal of Oral Glucose in Man. Diabetes. 1983;32:675–9.
15. Topping DL, Mayes PA. The Concentrations of Fructose, Glucose and Lactate in the Splanchnic Blood Vessels of Rats Absorbing Fructose. Nutr Metabol. 1971;13:331–8.
16. Mendeloff AI, Weichselbaum TE. Role of the human liver in the assimilation of intravenously administered fructose. Metabolism. 1953;2:450–8.
17. Havel PJ. Dietary Fructose: Implications for Dysregulation of Energy Homeostasis and Lipid/Carbohydrate Metabolism. Nutr Rev. 2005;63:133–57.
18. Pilkis SJ, Granner DK. Molecular physiology of the regulation of hepatic gluconeogenesis and glycolysis. Annu Rev Physiol. 1992;54:885–909.
19. Printz RL, Magnuson MA, Granner DK. Mammalian glucokinase. Annu Rev Nutr. 1993;13:463–96.
20. Iynedjian PB, Jotterand D, Nouspikel T, Asfari M, Pilot P-R. Transcriptional Induction of Glucokinase Gene by Insulin in Cultured Liver Cells and Its Repression by the

Glucagon-CAMP System. J Biol Chem. 1989;264:21824–9.
21. Magnuson MA, Andreone TL, Printz RL, Koch S, Granner DK. Rat glucokinase gene: structure and regulation by insulin. Proc Natl Acad Sci USA. 1989;86:4838–42.
22. Van Schaftingen E. A protein from rat liver confers to glucokinase the property of being antagonistically regulated by fructose 6-phosphate and fructose 1-phosphate. Eur J Biochem. 1989;179:179–84.
23. Hers HG. La fructokinase du foie. Biochim Biophys Acta. 1952;8:416–23.
24. Renold AE, Hastings AB, Nesbett FB. Studies on carbohydrate metabolism in rat liver slices. III. Utilization of glucose and fructose by liver from normal and diabetic animals. J Biol Chem. 1954;209:687–96.
25. Adelman RC, Ballard FJ, Weinhouse S. Purification and Properties of Rat Liver Fructokinase. J Biol Chem. 1967;242:3360–5.
26. Underwood AH, Newsholme EA. Properties of Phosphofructokinase from Rat Liver and their Relation to the Control of Glycolysis and Gluconeogenesis. Biochem J. 1965;95:868–75.
27. Mayes PA. Intermediary metabolism of fructose. Am J Clin Nutr. 1993;58:754S-765S.
28. Softic S, Cohen, Cohen DE, Kahn CR. Role of Dietary Fructose and Hepatic de novo Lipogenesis in Fatty Liver Disease. Dig Dis Sci. 2016;61:1282–1293.
29. Miller M, Drucker WR, Owens JE, Craig JW, Woodward HJr. Metabolism of intravenous fructose and glucose in normal and diabetic subjects. J Clin Invest. 1952;31:115–25.
30. Bode JCh, Zelder O, Rumpelt HJ, Wittkamp U. Depletion of Liver Adenosine Phosphates and Metabolic Effects of Intravenous Infusion of Fructose or Sorbitol in Man and in the Rat. Europ J clin Invest. 1973;3:436–41.
31. Zakim D, Pardini RS, Herman RH, Sauberlich HE. Mechanism for the differential effects of high carbohydrate diets on lipogenesis in rat liver. Biochim Biophys Acta. 1967;144:242–51.
32. Kim M-S, Krawczyk SA, Doridot L, Fowler AJ, Wang JX, Trauger SA, Noh H-L, Kang HJ, Meissen JK, Blatnik M, et al. ChREBP regulates fructose-induced glucose production independently of insulin signaling. J Clin Invest. 2016;126:4372–86.
33. Softic S, Gupta MK, Wang G-X, Fujisaka S, O'Neill BT, Rao TN, Willoughby J, Harbison C, Fitzgerald K, Ilkayeva O, et al. Divergent effects of glucose and fructose on hepatic lipogenesis and insulin signaling. J Clin Invest. 2017;127:4059–74.
34. Bode C, Dürr H-K, Bode JC. Effect of fructose feeding on the activity of enzymes of glycolysis, gluconeogenesis, and the pentose phosphate shunt in the liver and jejunal mucosa of rats. Horm Metab Res. 1981;13:379–83.
35. Roglans N, Vila L, Farre M, Alegret M, Sanchez RM, Vazquez-Carrera M, Laguna JC. Impairment of Hepatic Stat-3 Activation and Reduction of PPAR Alpha Activity in Fructose-Fed Rats. Hepatology. 2007;45:778–88.
36. Stanhope KL, Schwarz JM, Keim NL, Griffen SC, Bremer AA, Graham JL, Hatcher B, Cox CL, Dyachenko A, Zhang W, et al. Consuming fructose-sweetened, not glucose-sweetened, beverages increases visceral adiposity and lipids and decreases insulin sensitivity in overweight/obese humans. J Clin Invest. 2009;119:1322–34.
37. Cox CL, Stanhope KL, Schwarz JM, Graham JL, Hatcher B, Griffen SC, Bremer AA, Berglund L, McGahan JP, Havel PJ, et al. Consumption of fructose-sweetened beverages for 10 weeks reduces net fat oxidation and energy expenditure in overweight/obese men and women. Eur J Clin Nutr. 2012;66:201–8.
38. Cox CL, Stanhope KL, Schwarz JM, Graham JL, Hatcher B, Griffen SC, Bremer AA, Berglund L, McGahan JP, Keim NL, et al. Circulating Concentrations of Monocyte Chemoattractant Protein-1, Plasminogen Activator Inhibitor-1, and Soluble Leukocyte Adhesion Molecule-1 in Overweight/Obese Men and Women Consuming Fructose- or

Glucose-Sweetened Beverages for 10 Weeks. J Clin Endocrinol Metab. 2011;96:E2034–8.
39. Mäenpää PH, Raivio KO, Kekomäki MP. Liver adenine nucleotides: fructose-induced depletion and its effect on protein synthesis. Science. 1968;161:1253–4.
40. Perheentupa J, Raivio K. Fructose-induced hyperuricaemia. Lancet. 1967;290:528–31.
41. Lanaspa MA, Sanchez-Lozada LG, Choi Y-J, Cicerchi C, Kanbay M, Roncal-Jimenez CA, Ishimoto T, Li N, Marek G, Duranay M, et al. Uric acid induces hepatic steatosis by generation of mitochondrial oxidative stress: potential role in fructose-dependent and -independent fatty liver. J Biol Chem. 2012;287:40732–44.
42. Choi Y-J, Shin H-S, Choi HS, Park J-W, Jo I, Oh E-S, Lee K-Y, Lee B-H, Johnson RJ, Kang D-H. Uric acid induces fat accumulation via generation of endoplasmic reticulum stress and SREBP-1c activation in hepatocytes. Laboratory Investigation. 2014;94:1114–25.
43. Zhang C, Chen X, Zhu R-M, Zhang Y, Yu T, Wang H, Zhao H, Zhao M, Ji Y-L, Chen Y-H, et al. Endoplasmic reticulum stress is involved in hepatic SREBP-1c activation and lipid accumulation in fructose-fed mice. Toxicology Letters. 2012;212:229–40.
44. Lee A-H, Scapa EF, Cohen DE, Glimcher LH. Regulation of hepatic lipogenesis by the transcription factor XBP1. Science. 2008;320:1492–1496.
45. Puri P, Baillie RA, Wiest MM, Mirshahi F, Choudhury J, Cheung O, Sargeant C, Contos MJ, Sanyal AJ. A Lipidomic Analysis of Nonalcoholic Fatty Liver Disease. Hepatology. 2007;46:1081–90.
46. Jornayvaz FR, Shulman GI. Diacylglycerol Activation of Protein Kinase Cε and Hepatic Insulin Resistance. Cell Metab. 2012;15:574–84.
47. Tobey TA, Mondon CE, Zavaroni I, Reaven GM. Mechanism of insulin resistance in fructose-fed rats. Metabolism. 1982;31:608–12.
48. Aeberli I, Hochuli M, Gerber PA, Sze L, Murer SB, Tappy L, Spinas GA, Berneis K. Moderate Amounts of Fructose Consumption Impair Insulin Sensitivity in Healthy Young Men. Diabetes Care. 2013;36:150–6.
49. Faeh D, Minehira K, Schwarz J-M, Periasami R, Seongsu P, Tappy L. Effect of Fructose Overfeeding and Fish Oil Administration on Hepatic De Novo Lipogenesis and Insulin Sensitivity in Healthy Men. Diabetes. 2005;54:1907–13.
50. Aeberli I, Gerber PA, Hochuli M, Kohler S, Haile SR, Gouni-Berthold I, Berthold HK, Spinas GA, Berneis K. Low to moderate sugar-sweetened beverage consumption impairs glucose and lipid metabolism and promotes inflammation in healthy young men: a randomized controlled trial. Am J Clin Nutr. 2011;94:85–479.
51. Jin R, Vos MB. Fructose and liver function – is this behind nonalcoholic liver disease? Curr Opin Clin Nutr Metab Care. 2015;18:490–5.
52. Bergheim I, Weber S, Vos M, Krämer S, Volynets V, Kaserouni S, McClain CJ, Bischoff SC. Antibiotics protect against fructose-induced hepatic lipid accumulation in mice: role of endotoxin. J Hepatol. 2008;48:983–92.
53. Kanuri G, Spruss A, Wagnerberger S, Bischoff SC, Bergheim I. Role of tumor necrosis factor α (TNFα) in the onset of fructose-induced nonalcoholic fatty liver disease in mice. J Nutr Biochem. 2011;22:527–34.
54. Spruss A, Kanuri G, Wagnerberger S, Haub S, Bischoff SC, Bergheim I. Toll-like receptor 4 is involved in the development of fructose-induced hepatic steatosis in mice. Hepatology. 2009;50:1094–104.
55. Spruss A, Bergheim I. Dietary fructose and intestinal barrier: potential risk factor in the pathogenesis of nonalcoholic fatty liver disease. J Nutr Biochem. 2009;20:657–62.
56. Brandt A, Nier A, Jin CJ, Baumann A, Jung F, Ribas V, Garcia-Ruiz C, Fernandez-Checa JC, Bergheim I. Consumption of decaffeinated coffee protects against the development of T early non-alcoholic steatohepatitis: Role of intestinal barrier function. Redox Biology. 2019;21:101092.
57. Ritze Y, Bárdos G, Claus A, Ehrmann V, Bergheim I, Schwiertz A, Bischoff SC.

Lactobacillus rhamnosus GG protects against non-alcoholic fatty liver disease in mice. PLoS ONE. 2014;9:e80169.
58. Wagnerberger S, Spruss A, Kanuri G, Stahl C, Schröder M, Vetter W, Bischoff SC, Bergheim I. Lactobacillus casei Shirota protects from fructose-induced liver steatosis: A mouse model. J Nutr Biochem. 2013;24:531–8.
59. Volynets V, Spruss A, Kanuri G, Wagnerberger S, Bischoff SC, Bergheim I. Protective effect of bile acids on the onset of fructose-induced hepatic steatosis in mice. J Lipid Res. 2010;51:3414–24.
60. Sen T, Cawthon CR, Ihde BT, Hajnal A, DiLorenzo PM, de La Serre CB, Czaja K. Diet-driven microbiota dysbiosis is associated with vagal remodeling and obesity. Physiol Behav. 2017;173:305–17.
61. Hunnisett A, Howard J, Davies S. Gut Fermentation (or the 'Auto-brewery') Syndrome: A New Clinical Test with Initial Observations and Discussion of Clinical and Biochemical Implications. Journal of Nutritional Medicine. 1990;1:33–8.
62. Zhu L, Baker SS, Gill C, Liu W, Alkhouri R, Baker RD, Gill SR. Characterization of Gut Microbiomes in Nonalcoholic Steatohepatitis (NASH) Patients: A Connection Between Endogenous Alcohol and NASH. Hepatology. 2013;57:601–9.
63. Bode C, Kugler V, Bode JC. Endotoxemia in patients with alcoholic and non-alcoholic cirrhosis and in subjects with no evidence of chronic liver disease following acute alcohol excess. J Hepatol. 1987;4:8–14.
64. Volynets V, Louis S, Pretz D, Lang L, Ostaff MJ, Wehkamp J, Bischoff SC. Intestinal Barrier Function and the Gut Microbiome Are Differentially Affected in Mice Fed a Western-Style Diet or Drinking Water Supplemented with Fructose. J Nutr. 2017;147:770–80.
65. Kirpich IA, Marsano LS, McClain CJ. Gut-Liver Axis, Nutrition, and Non Alcoholic Fatty Liver Disease. Clin Biochem. 2016;48:923–930.
66. Haub S, Kanuri G, Volynets V, Brune T, Bischoff SC, Bergheim I. Serotonin reuptake transporter (SERT) plays a critical role in the onset of fructose-induced hepatic steatosis in mice. Am J Physiol Gastrointest Liver Physiol. 2010;298:G335–G344.
67. Wagnerberger S, Spruss A, Kanuri G, Volynets V, Stahl C, Bischoff SC, Bergheim I. Toll-like receptors 1–9 are elevated in livers with fructose-induced hepatic steatosis. Br J Nutr. 2012;107:1727–1738.
68. Nier A, Brandt A, Rajcic D, Bruns T, Bergheim I. Short-Term Isocaloric Intake of a Fructose- but not Glucose-Rich Diet Affects Bacterial Endotoxin Concentrations and Markers of Metabolic Health in Normal Weight Healthy Subjects. Molecular Nutrition & Food Research. 2018;
69. Shen P, Yue Y, Park Y. A living model for obesity and aging research: Caenorhabditis elegans. Crit Rev Food Sci Nutr. 2018;58:741–54.
70. Zheng J, Greenway FL. Caenorhabditis elegans as a model for obesity research. Int J Obes (Lond). 2012;36:186–94.
71. Corsi AK. A Transparent window into biology: A primer on Caenorhabditis elegans. WormBook. 2015;1–31.
72. Corsi AK. A biochemist's guide to Caenorhabditis elegans. Anal Biochem. 2006;359:1–17.
73. Lemieux GA, Liu J, Mayer N, Bainton RJ, Ashrafi K, Werb Z. A whole-organism screen identifies new regulators of fat storage. Nat Chem Biol. 2011;7:206–13.
74. Jones KT, Ashrafi K. Caenorhabditis elegans as an emerging model for studying the basic biology of obesity. DMM. 2009;2:224–9.
75. O'Rourke EJ, Soukas AA, Carr CE, Ruvkun G. C. elegans major fats are stored in vesicles distinct from lysosome-related organelles. Cell Metab. 2009;10:430–5.
76. Ashrafi K. Obesity and the regulation of fat metabolism. WormBook. 2007;1–20.
77. Mak HY. Lipid droplets as fat storage organelles in Caenorhabditis elegans: Thematic

Review Series: Lipid Droplet Synthesis and Metabolism: from Yeast to Man. J Lipid Res. 2012;53:28–33.
78. Lemieux GA, Ashrafi K. Insights and challenges in using C. elegans for investigation of fat metabolism. Crit Rev Biochem Mol Biol. 2015;50:69–84.
79. Hench J, Bratić Hench I, Pujol C, Ipsen S, Brodesser S, Mourier A, Tolnay M, Frank S, Trifunović A. A tissue-specific approach to the analysis of metabolic changes in Caenorhabditis elegans. PLoS ONE. 2011;6:e28417.
80. Brooks KK, Liang B, Watts JL. The influence of bacterial diet on fat storage in C. elegans. PLoS ONE. 2009;4:e7545.
81. Perez CL, Van Gilst MR. A 13C isotope labeling strategy reveals the influence of insulin signaling on lipogenesis in C. elegans. Cell Metab. 2008;8:266–74.
82. Zhang SO, Trimble R, Guo F, Mak HY. Lipid droplets as ubiquitous fat storage organelles in C. elegans. BMC Cell Biol. 2010;11:96.
83. Zhang SO, Box AC, Xu N, Le Men J, Yu J, Guo F, Trimble R, Mak HY. Genetic and dietary regulation of lipid droplet expansion in Caenorhabditis elegans. Proc Natl Acad Sci USA. 2010;107:4640–5.
84. Hellerer T, Axäng C, Brackmann C, Hillertz P, Pilon M, Enejder A. Monitoring of lipid storage in Caenorhabditis elegans using coherent anti-Stokes Raman scattering (CARS) microscopy. Proc Natl Acad Sci USA. 2007;104:14658–63.
85. Altun ZF, Hall DH. Alimentary system, overview. WormAtlas. 2009;
86. Altun ZF, Hall DH. Alimentary system, intestine. WormAtlas. 2009;
87. Stiernagle T. Maintenance of C. elegans. WormBook [Internet]. 2006 [cited 2018 Jun 25]; Available from: http://www.wormbook.org/chapters/www_strainmaintain/strainmaintain.html
88. Cabreiro F, Gems D. Worms need microbes too: microbiota, health and aging in Caenorhabditis elegans. EMBO Mol Med. 2013;5:1300–10.
89. Gusarov I, Gautier L, Smolentseva O, Shamovsky I, Eremina S, Mironov A, Nudler E. Bacterial Nitric Oxide extends the lifespan of C. elegans. Cell. 2013;152:818–30.
90. Maier W, Adilov B, Regenass M, Alcedo J. A Neuromedin U Receptor Acts with the Sensory System to Modulate Food Type-Dependent Effects on C. elegans Lifespan. PLoS Biology. 2010;8:1–18.
91. Pásti G, Labouesse M. Epithelial junctions, cytoskeleton, and polarity. WormBook. 2014;1–35.
92. Günzel D, Yu ASL. Claudins and the modulation of tight junction permeability. Physiol Rev. 2013;93:525–69.
93. Furuse M, Hata M, Furuse K, Yoshida Y, Haratake A, Sugitani Y, Noda T, Kubo A, Tsukita S. Claudin-based tight junctions are crucial for the mammalian epidermal barrier: a lesson from claudin-1–deficient mice. J Biol Chem. 2002;156:1099–111.
94. Asano A, Asano K, Sasaki H, Furuse M, Tsukita S. Claudins in Caenorhabditis elegans: their distribution and barrier function in the epithelium. Curr Biol. 2003;13:1042–6.
95. Fanning AS, Jameson BJ, Jesaitis LA, Anderson JM. The Tight Junction Protein ZO-1 Establishes a Link between the Transmembrane Protein Occludin and the Actin Cytoskeleton. J Biol Chem. 1998;273:29745–53.
96. Fanning AS, Anderson JM. Zonula Occludens-1 and -2 Are Cytosolic Scaffolds That Regulate the Assembly of Cellular Junctions. Ann N Y Acad Sci. 2009;113–120.
97. Lockwood C, Zaidel-Bar R, Hardin J. The C. elegans zonula occludens ortholog cooperates with the cadherin complex to recruit actin during morphogenesis. Curr Biol. 2008;18:1333–7.
98. Ng M, Fleming T, Robinson M, Thomson B, Graetz N, Margono C, Mullany EC, Biryukov S, Abbafati C, Abera SF. Global, regional and national prevalence of overweight and obesity in children and adults 1980-2013: A systematic analysis. Lancet. 2014;384:766–

81.
99. Yach D, Hawkes C, Gould CL, Hofman KJ. The Global Burden of Chronic Diseases: Overcoming Impediments to Prevention and Control. JAMA. 2004;291:2616–22.
100. Younossi ZM, Koenig AB, Abdelatif D, Fazel Y, Henry L, Wymer M. Global Epidemiology of Nonalcoholic Fatty Liver Disease—Meta-Analytic Assessment of Prevalence, Incidence, and Outcomes. Hepatology. 2016;64.
101. Chalasani N, Younossi Z, Lavine JE, Charlton M, Cusi K, Rinella M, Harrison SA, Brunt EM, Sanyal AJ. The Diagnosis and Management of Nonalcoholic Fatty Liver Disease: Practice Guidance From the American Association for the Study of Liver Diseases. Hepatology. 2018;67:328–57.
102. Musso G, Cassader M, Rosina F, Gambino R. Impact of current treatments on liver disease, glucose metabolism and cardiovascular risk in non-alcoholic fatty liver disease (NAFLD): a systematic review and meta-analysis of randomised trials. Diabetologia. 2012;55:885–905.
103. Do MH, Lee E, Oh M-J, Kim Y, Park H-Y. High-Glucose or -Fructose Diet Cause Changes of the Gut Microbiota and Metabolic Disorders in Mice without Body Weight Change. Nutrients. 2018;10:1–14.
104. Brenner S. The genetics of Caenorhabditis elegans. Genetics. 1974;77:71–94.
105. Weimer S, Priebs J, Kuhlow D, Groth M, Priebe S, Mansfeld J, Merry TL, Dubuis S, Laube B, Pfeiffer AF, et al. D-Glucosamine supplementation extends life span of nematodes and of ageing mice. Nat Commun. 2014;5:1–12.
106. Ogawa A, Sommer RJ. Developmental biology. Strategies to get arrested. Science. 2009;326:944–5.
107. Corsi AK, Wightman B, Chalfie M. A Transparent window into biology: A primer on Caenorhabditis elegans. WormBook. 2015;1–31.
108. Folch J, Lees M, Sloane Stanley GH. A simple method for the isolation and purification of total lipides from animal tissues. J Biol Chem. 1957;226:497–509.
109. Fossati P, Prencipe L. Serum triglycerides determined colorimetrically with an enzyme that produces hydrogen peroxide. Clin Chem. 1982;28:2077–80.
110. Bradford MM. A rapid and sensitive method for the quantitation of microgram quantities of protein utilizing the principle of protein-dye binding. Anal Biochem. 1976;72:248–54.
111. Compton SJ, Jones CG. Mechanism of dye response and interference in the Bradford protein assay. Anal Biochem. 1985;151:369–74.
112. Heestand BN, Shen Y, Liu W, Magner DB, Storm N, Meharg C, Habermann B, Antebi A. Dietary restriction induced longevity is mediated by nuclear receptor NHR-62 in Caenorhabditis elegans. PLoS Genet. 2013;9:e1003651.
113. Wählby C, Conery AL, Bray M-A, Kamentsky L, Larkins-Ford J, Sokolnicki KL, Veneskey M, Michaels K, Carpenter AE, O'Rourke EJ. High- and low-throughput scoring of fat mass and body fat distribution in C. elegans. Methods. 2014;68:492–9.
114. Escorcia W, Ruter DL, Nhan J, Curran SP. Quantification of Lipid Abundance and Evaluation of Lipid Distribution in Caenorhabditis elegans by Nile Red and Oil Red O Staining. J Vis Exp. 2018;e57352.
115. Gelino S, Chang JT, Kumsta C, She X, Davis A, Nguyen C, Panowski S, Hansen M. Intestinal Autophagy Improves Healthspan and Longevity in C. elegans during Dietary Restriction. PLoS Genet. 2016;12:e1006135.
116. Rera M, Bahadorani S, Cho J, Koehler CL, Ulgherait M, Hur JH, Ansari WS, Lo TJr, Jones DL, Walker DW. Modulation of Longevity and Tissue Homeostasis by the Drosophila PGC-1 Homolog. Cell Metab. 2011;14:623–34.
117. Rera M, Clark RI, Walker David W. Intestinal barrier dysfunction links metabolic and inflammatory markers of aging to death in Drosophila. Proc Natl Acad Sci U S A.

2012;109:21528–33.
118. Chomczynski P, Sacchi N. The single-step method of RNA isolation by acid guanidinium thiocyanate-phenol-chloroform extraction: twenty-something years on. Nat Protoc. 2006;1:581–5.
119. Desjardins P, Conklin D. NanoDrop microvolume quantitation of nucleic acids. J Vis Exp. 2010;45:e2565.
120. Schmittgen TD, Zakrajsek BA, Mills AG, Gorn V, Singer MJ, Reed MW. Quantitative Reverse Transcription–Polymerase Chain Reaction to Study mRNA Decay: Comparison of Endpoint and Real-Time Methods. Analytical Biochemistry. 2000;285:194–204.
121. Livak KJ, Schmittgen TD. Analysis of relative gene expression data using real-time quantitative PCR and the 2(-Delta Delta C(T)) Method. Methods. 2001;25:402–8.
122. Jegatheesan P, De Bandt J-P.
Fructose and NAFLD: The Multifaceted Aspects of Fructose Metabolism. Nutrients. 2017;9.
123. Sellmann C, Priebs J, Landmann M, Degen C, Engstler AJ, Jin CJ, Gärttner S, Spruss A, Huber O, Bergheim I. Diets rich in fructose, fat or fructose and fat alter intestinal barrier function and lead to the development of nonalcoholic fatty liver disease over time. J Nutr Biochem. 2015;26:1183–92.
124. Jena PK, Singh S, Prajapati B, Nareshkumar G, Mehta T, Seshadri S. Impact of targeted specific antibiotic delivery for gut microbiota modulation on high-fructose-fed rats. Appl Biochem Biotechnol. 2014;172:3810–26.
125. Di Luccia B, Crescenzo R, Mazzoli A, Cigliano L, Venditti P, Walser J-C, Widmer A, Baccigalupi L, Ricca E, Iossa S. Rescue of Fructose-Induced Metabolic Syndrome by Antibiotics or Faecal Transplantation in a Rat Model of Obesity. PLoS One. 2015;10:e0134893.
126. Alcántar-Fernández J, Navarro RE, Salazar-Martínez AM, Pérez-Andrade ME, Miranda-Ríos J. Caenorhabditis elegans respond to high-glucose diets through a network of stress-responsive transcription factors. PLoS ONE. 2018;13:e0199888.
127. Lee S-J, Murphy CT, Kenyon C. Glucose shortens the life span of C. elegans by downregulating DAF-16/FOXO activity and aquaporin gene expression. Cell Metab. 2009;10:379–91.
128. Mondoux MA, Love DC, Ghosh SK, Fukushige T, Bond M, Weerasinghe GR, Hanover JA, Krause MW. O-Linked-N-Acetylglucosamine Cycling and Insulin Signaling Are Required for the Glucose Stress Response in Caenorhabditis elegans. Genetics. 2011;188:369–382.
129. Schulz TJ, Zarse K, Voigt A, Urban N, Birringer M, Ristow M. Glucose Restriction Extends Caenorhabditis elegans Life Span by Inducing Mitochondrial Respiration and Increasing Oxidative Stress. Cell Metab. 2007;6:280–293.
130. Tauffenberger A, Vaccaro A, Aulas A, Vande Velde C, Parker JA. Glucose delays age-dependent proteotoxicity. Aging Cell. 2012;11:856–66.
131. Zheng J, Gao C, Wang M, Tran P, Mai N, Finley JW, Heymsfield SB, Greenway FL, Li Z, Heber D, et al. Lower Doses of Fructose Extend Lifespan in Caenorhabditis elegans. J Diet Suppl. 2017;14:264–77.
132. Gems D, Riddle DL. Defining Wild-Type Life Span in Caenorhabditis elegans. J Gerontol A Biol Sci Med Sci. 2000;55:B215–B219.
133. Clark LC, Hodgkin J. Commensals, probiotics and pathogens in the Caenorhabditis elegans model. Cell Microbiol. 2014;16:27–38.
134. Fraenkel DG. The Phosphoenolpyruvate-initiated Pathway of Fructose Metabolism in Escherichia coli. The Journal of Biological Chemistry. 1968;243:6458–63.
135. Soukas AA, Kane EA, Carr CE, Melo JA, Ruvkun G. Rictor/TORC2 regulates fat metabolism, feeding, growth, and life span in Caenorhabditis elegans. Genes & Dev. 2009;23:496–511.

136. Kim JI, Huh JY, Sohn JH, Choe SS, Lee YS, Lim CY, Jo A, Park SB, Han W, Kim JB. Lipid-overloaded enlarged adipocytes provoke insulin resistance independent of inflammation. Mol Cell Biol. 2015;35:1686–99.
137. Sanjabi B, Dashty M, Özcan B, Akbarkhanzadeh V, Rahimi M, Vinciguerra M, van Rooij F, Al-Lahham S, Sheedfar F, van Kooten TG, et al. Lipid droplets hypertrophy: a crucial determining factor in insulin regulation by adipocytes. Sci Rep. 2015;5:8816.
138. Pukkila-Worley R, Ausubel FM. Immune defense mechanisms in the Caenorhabditis elegans intestinal epithelium. Curr Opin Immunol. 2012;24:3–9.
139. Dambroise E, Monnier L, Ruisheng L, Aguilaniu H, Joly J-S, Tricoire H, Rera M. Two phases of aging separated by the Smurf transition as a public path to death. Sci Rep. 2016;6:1–7.
140. Martins RR, McCracken AWW, Simons MJP, Henriques CMM, Rera M. How to Catch a Smurf? – Ageing and Beyond... In vivo Assessment of Intestinal Permeability in Multiple Model Organisms. Bio Protoc. 2018;8:pii: e2722.
141. Groschwitz KR, Hogan SP. Intestinal barrier function: molecular regulation and disease pathogenesis. J Allergy Clin Immunol. 2009;124:3–20; quiz 21–2.
142. Miele L, Valenza V, La Torre G, Montalto M, Cammarota G, Ricci R, Masciana R, Forgione A, Gabrieli ML, Perotti G, et al. Increased Intestinal Permeability and Tight Junction Alterations in Nonalcoholic Fatty Liver Disease. Hepatology. 2009;49:1877–87.
143. Lin J, Hackam D. Worms, flies and four-legged friends: the applicability of biological models to the understanding of intestinal inflammatory diseases. DMM. 2011;1–10.
144. Hulme SE, Whitesides GM. Chemistry and the worm: Caenorhabditis elegans as a platform for integrating chemical and biological research. Angew Chem Int Ed Engl. 2011;50:4774–807.
145. Baena M, Sangüesa G, Dávalos A, Latasa M-J, Sala-Vila A, Sánchez RM, Roglans N, Laguna JC, Alegret M. Fructose, but not glucose, impairs insulin signaling in the three major insulin-sensitive tissues. Sci Rep. 2016;6:26149.
146. Mastrocola R, Ferrocino I, Liberto E, Chiazza F, Cento A, Collotta D, Querio G, Nigro D, Bitonto V, Cutrin J, et al. Fructose liquid and solid formulations differently affect gut integrity, microbiota composition and related liver toxicity: a comparative in vivo study. J Nutr Biochem. 2018;55:185–99.